Japan Architectural Review
Open Access
Architectural Institute of Japan

Original Paper

Seismic performance of buckling-restrained brace outrigger system in various configurations

Pao-Chun Lin and Toru Takeuchi

Department of Architecture and Building Engineering, Tokyo Institute of Technology, Meguro-ku, Tokyo, Japan

Correspondence
Toru Takeuchi, Department of Architecture and Building Engineering, Tokyo Institute of Technology, Meguro-ku, Tokyo, Japan.
Email: takeuchi.t.ab@m.titech.ac.jp

Funding information
Japan Society for the Promotion of Science, Grant/Award Number: 18J15047

Received March 5, 2019; Accepted July 16, 2019

doi: 10.1002/2475-8876.12120

Abstract

The outrigger system is deemed an effective solution for mitigating the seismic responses of tall core-tube-type buildings. By incorporating a buckling-restrained brace (BRB) in the outrigger system (BRB-outrigger), the BRB-outrigger reduces seismic response not only through the outrigger mechanism but also through the seismic energy dissipation from the BRB's hysteretic response. This study investigates the seismic behavior of structures with a single layer BRB-outrigger and proposes three types of BRB-outrigger configurations for practical design purposes that fit different architectural requirements. An analytical model, with heights of 64, 128, 256, and 384 m and different outrigger spans was used to investigate the optimal outrigger elevation and required outrigger stiffness for achieving minimum seismic response using spectral analysis and nonlinear response history analysis. The design indexes and design charts based on the analysis results are proposed for preliminary design. Design examples of structures with different BRB-outrigger configurations utilizing the proposed design charts are demonstrated.

Keywords
buckling-restrained brace, optimal design, outrigger, parametric study, spectral analysis

1. Introduction

The outrigger system has been an effective solution in tall core-tube-type buildings for mitigating seismic responses, and it has been widely adopted in tall buildings worldwide.[1] When lateral loads are applied, the relatively stiff outrigger, which connects the core structure and the perimeter column, applies a resisting moment to the core structure to reduce roof drift, inter-story drift, and bending moment of the core structure.[2] The design of the conventional outrigger that allows for all members to be elastic could be uneconomical. Therefore, the concept of a damped-outrigger was proposed.[3] The most common damped-outrigger configuration has the dampers inserted at the outrigger truss end and the perimeter column. The dampers dissipate energy through relative movements between the outrigger truss end and the perimeter column.[4] This damped-outrigger configuration incorporating viscous dampers has been used in studies[5,6] to investigate optimal outrigger elevation to maximize the system damping ratio. The study[5] indicates that the elevation of optimal damped-outrigger when viscous dampers are incorporated ranges from 50% to 80% of the building height. The damped-outrigger system incorporating viscous dampers has also been utilized in real construction projects to reduce wind load effect.[7] The damped-outrigger incorporating a buckling-restrained brace (BRB)[8] as the energy dissipation device has also been studied.[9] The damped-outrigger incorporating a BRB (BRB-outrigger) functions as a conventional outrigger system during small earthquakes, and the BRB deforms elastically. During large earthquakes, the BRB dissipates seismic energy through its hysteretic response. Furthermore, the BRB can limit the maximum force demands on the perimeter column and the outrigger truss members. The arrangement of a BRB to function as an outrigger has also been adopted in real construction project.[10] Most of the studies that investigate optimal outrigger elevations were determined using preselected possible elevations. The continuous seismic response distributions with respect to changes in outrigger elevation have not been demonstrated. Furthermore, the details of BRB-outrigger configurations to fit different architectural requirements have not been proposed.

Figure 1 shows a laterally deformed structure with a BRB-outrigger. The core structure provides most of the lateral stiffness and lateral force resistance capacity. The BRB is arranged vertically between the outrigger truss ends and the perimeter columns to optimally impose axial deformation demand on the BRB. As shown in Figure 1, when the structure deforms laterally to the right, the BRB and perimeter column on the right-hand side are in compression, and in tension on the left-hand

side. The outrigger truss, BRB, and perimeter columns act in series to provide a resisting moment to the core structure. When the BRB yields, the BRB starts dissipating energy. The maximum force demands for the outrigger truss members and perimeter columns are limited by the maximum axial force developed in the BRBs. However, when the outrigger span is long, the relative movement between the outrigger truss end and the perimeter becomes very large. Therefore, the BRB length should be very long (8-10 m) to meet the large deformation demand. Furthermore, the design of the outrigger truss is sometimes difficult and uneconomical because very large sections of the outrigger truss members are required to make the outrigger sufficiently stiff. These shortcomings could make a BRB-outrigger system solution an uneconomical and impractical seismic design solution.

With this background, the aim of this research was to introduce alternative BRB-outrigger configurations for achieving economical and effective design results. The indexes of the stiffness provided by the BRB-outrigger to the core structure's rotational stiffness, and to the perimeter column axial stiffness are introduced for comparison for seismic performance between structures with different BRB-outrigger configurations. These indexes and the outrigger elevation for minimizing seismic response were investigated. This study uses a simplified structure and increases the number of analytical models with different heights (64, 128, 256, and 384 m) and outrigger spans (12.8, 13.8, 14.5, and 16 m) for enhanced verification of optimal design results. The continuous seismic response distributions with respect to various outrigger elevations and different outrigger stiffness are demonstrated by performing spectral analysis (SA) and nonlinear response history analysis (NLRHA). The maximum roof drift ratio and the base overturning moment at the core structure base are adopted as seismic performance indicators. The optimal outrigger elevations in order to maximize outrigger effect, maximize BRB energy dissipation efficiency, and minimize roof drift ratio and base overturning moment responses are investigated. Design charts based on newly introduced design indexes are proposed to assist designers with selecting an appropriate outrigger elevation and determining the required outrigger stiffness at the preliminary design stage. Furthermore, three different BRB-outrigger configurations are proposed in this research. Methods for using the simplified structure to model structures with different BRB-outrigger configurations are proposed. Based on the analysis results, all three BRB-outrigger configurations are capable of achieving the desired seismic response. The suitability of each BRB-outrigger configuration for different architectural requirements is discussed.

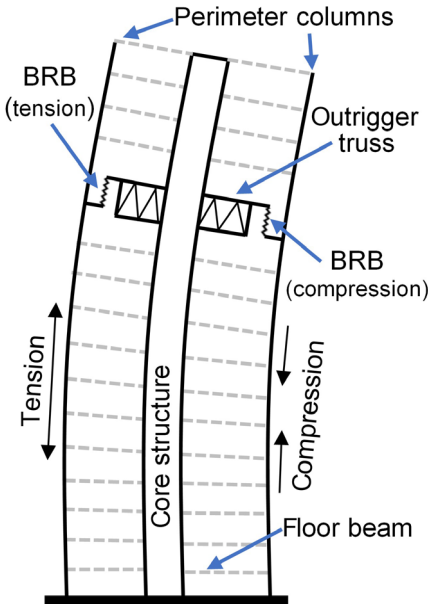

Figure 1. Deformed structure with BRB-outrigger system

2. Numerical Model

The structure with a single ordinary BRB-outrigger system (OB outrigger) can be simplified, as shown in Figure 2A. The core structure, which provides most of the lateral stiffness, is modeled using a cantilever column with a lateral flexural stiffness of EI. The outrigger truss has a flexural stiffness of k_t. The perimeter column with a length of h has an axial stiffness of k_c. The bases of the perimeter columns are free to rotate about the out-of-plane direction. The BRB has a bilinear force-deformation relationship with an axial initial stiffness of k_d and a post-yield stiffness ratio of 0.01. Each of the BRB connects to the outrigger truss end and perimeter column with pinned-connection detail. For simplicity, in this simplified model, it is assumed that only the BRBs can yield while the other elements deform elastically. The mass is assumed to be concentrated at the core structure and uniformly distributed along the core structure height. As shown in Figure 2A, if θ_1 is the core structure rotation at an outrigger elevation of α, the relationship between θ_1 and the flexural deformation of the outrigger truss (u_t), axial deformations of the BRB (u_d), and perimeter column below the outrigger elevation (u_c) is expressed as follows:

$$\theta_1 = \frac{1}{l_t}(u_c + u_t + u_d) \tag{1}$$

Therefore, the moment applied by the OB outrigger ($M_{o,OB}$) is calculated as follows:

$$M_{o,OB} = \frac{2l_t^2}{\alpha/k_c + 1/k_d + 1/k_t}\theta_1 = \frac{2l_t^2}{\alpha/k_c + 1/k_{og,OB}}\theta_1 = k_{rg,OB}\theta_1 \tag{2}$$

where l_t and $k_{rg,OB}$ are the outrigger span and the rotational stiffness provided by the OB outrigger system, respectively. $k_{og,OB}$ $(1/(1/k_d + 1/k_t))$, including the elastic stiffness of the BRB, is defined as the outrigger stiffness, which is the combined stiffness of k_d and k_t in the OB outrigger configuration. When the BRB yields, the corresponding core structure rotation at outrigger elevation θ_y can be calculated as follows:

$$\theta_y = \frac{k_d}{l_t}\left(\frac{\alpha}{k_c} + \frac{1}{k_t} + \frac{1}{k_d}\right)u_{d,y} = \frac{k_d}{l_t}\left(\frac{\alpha}{k_c} + \frac{1}{k_{og,OB}}\right)u_{d,y} \tag{3}$$

where $u_{d,y}$ is the BRB yield deformation. Figure 2B shows an analytical model developed using OpenSees[11] to perform an analysis of a simplified structure with an outrigger. For simplicity, the BRB with a fixed length of 1 m is modeled using a truss element with bilinear material property. The post-yield stiffness ratio (p) is set as 0.01. The outrigger truss is modeled using an elastic beam column element, and its corresponding cross-sectional property is properly assigned so that its flexural stiffness is equal to k_t. The core structure is modeled using an

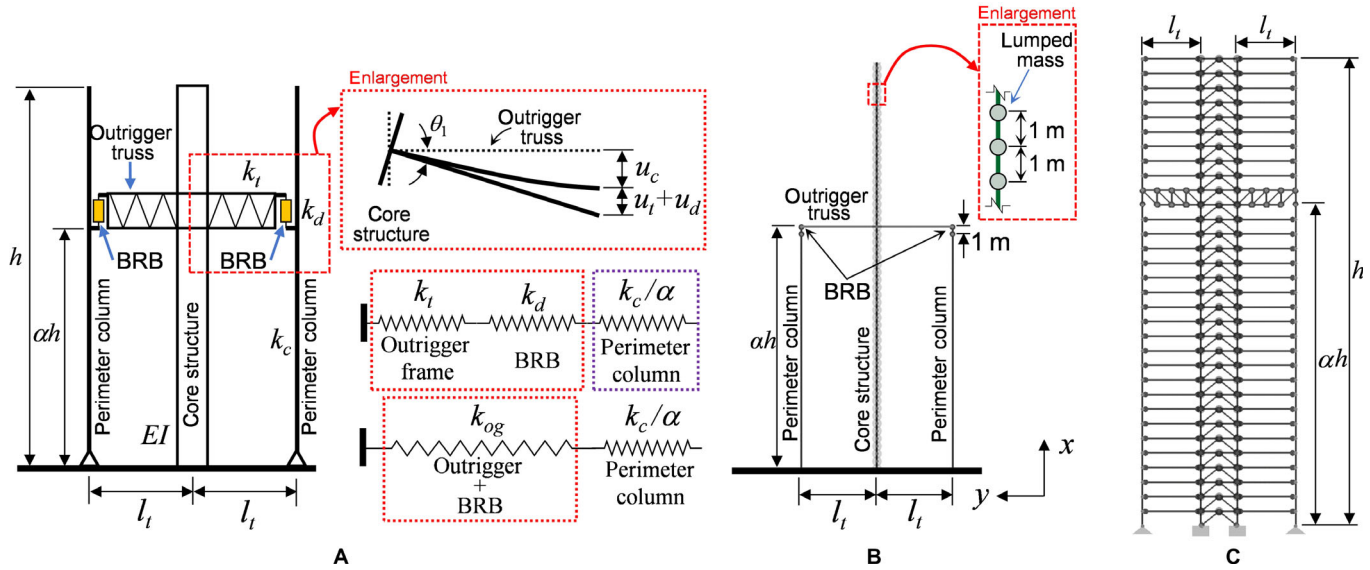

Figure 2. Simplified structure with (A) OB outrigger configuration (B) DM model (c) MBM model

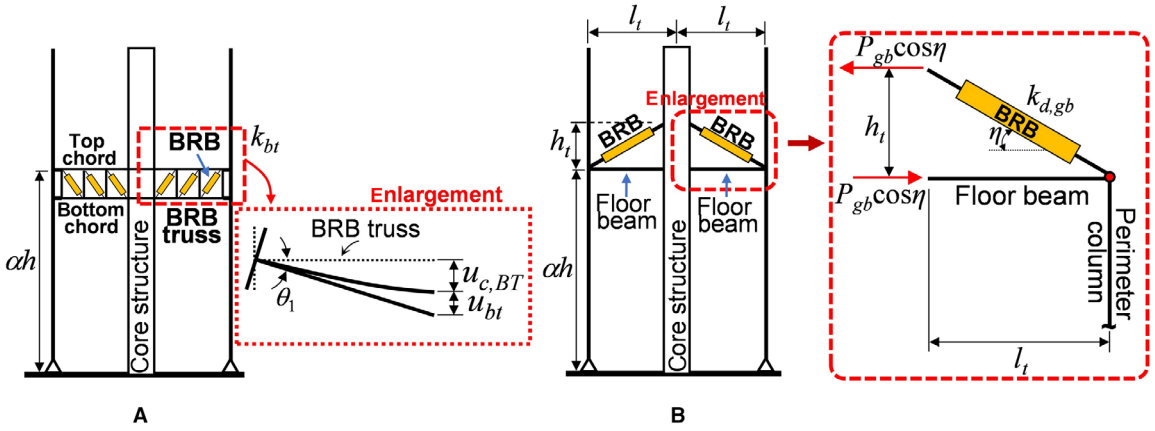

Figure 3. Configurations of the (A) BT outrigger system and (B) GB outrigger system

elastic beam column element. The mass is assigned to the nodes that evenly distribute along the core structure height with a fixed 1 m spacing. The core structure base is fixed, while the perimeter column bases are free to rotate about the z-axis. This model is known as a discrete mass (DM) model. The effectiveness of using a DM model to represent the real building was verified using a member-by-member (MBM) model, as shown in Figure 2C. Therefore, the BRB element in the MBM model is modeled by using bilinear material property. The core structure of the MBM model is represented by a braced frame. The mass is concentrated on each floor. The details of the floor beams and outrigger truss are all included in Figure 2C.

3. Configurations of BRB-Outrigger

In the OB outrigger configuration, the outrigger truss should be stiff enough to generate adequate axial deformation demand for the BRB. However, it would be difficult to design the outrigger truss members if l_t is too long or the desired k_t is too large. Furthermore, if the required BRB yield deformation (approximately 1/1000 of the BRB length) is large, the BRB length can be longer than one story height (Figure 18). To solve this problem, two alternative BRB-outrigger configurations are introduced.

Figure 3A shows the BRB-truss outrigger (BT outrigger) configuration. The BRBs are used as braces in the outrigger truss. The ends of the top and bottom chords that connect with the core structure and perimeter column can be designed with either shear or moment connection detail. As the BRBs and the outrigger truss members act in parallel, slight plastic deformation in the outrigger truss member may be allowed to prevent having too large an outrigger truss member size. When compared with the OB outrigger configuration, the outrigger truss member and BRB sizes can be reduced. Furthermore, the increased number of BRBs could provide a more stable energy dissipation mechanism. As shown in Figure 3A, the core structure rotation at outrigger elevation (θ_1) can be calculated as follows:

$$\theta_1 = \frac{1}{l_t}\left(u_{c,BT} + u_{bt}\right) \tag{4}$$

where $u_{c,BT}$ and u_{bt} are the perimeter column axial deformation and the flexural deformation of the BT outrigger, respectively.

Therefore, if k_{bt} is the flexural stiffness of the BT outrigger, the moment applied by the BT outrigger ($M_{o,BT}$) can be calculated as follows:

$$M_{o,BT} = \frac{2l_t^2}{\alpha/k_c + 1/k_{bt}}\theta_1 = \frac{2l_t^2}{\alpha/k_c + 1/k_{og,BT}}\theta_1 = k_{rg,BT}\theta_1 \quad (5)$$

where $k_{rg,BT}$ is the rotational stiffness provided by the BT outrigger system. When compared with Equation (2), the outrigger stiffness $k_{og,BT}$ is equal to k_{bt} in the BT outrigger configuration. If $u_{bt,y}$ is the BT outrigger flexural deformation when the first BRB yields, θ_y can be expressed as follows:

$$\theta_y = \frac{k_{bt}}{l_t}\left(\frac{\alpha}{k_c} + \frac{1}{k_{bt}}\right)u_{bt,y} \quad (6)$$

To use the DM model to analyze a structure with a BT outrigger, k_d, k_t, and $u_{d,y}$ in Equations (2) and (3) have to be replaced with k_{bt}, an infinity value, and $u_{bt,y}$, respectively.

Figure 3B shows the giant BRB-outrigger (GB outrigger) system. The GB outrigger removes the outrigger truss but connects the core structure and the perimeter column using a giant BRB. When a BRB axial force of P_{gb} is developed, the BRB and the floor beam below the BRB act as a force couple on the core structure, as shown in Figure 3B. The force couple applies a resisting moment ($M_{o,gb}$) to the core structure. It should be noted that both the BRB and floor beam are acting as truss elements. Furthermore, the floor beam is usually strong enough to resist the maximum force developed by the BRB and is stiff enough that the shortening or elongation of the floor beam can be neglected. If $u_{c,GB}$ and $u_{d,gb,v}$ are the vertical deformations of the perimeter column below the outrigger elevation and the BRB in the GB outrigger configuration (BRB_GB), and $k_{d,gb}$ is the axial stiffness of BRB_GB, the corresponding core structure rotation at outrigger elevation (θ_1) and $M_{o,gb}$ can be calculated as follows:

$$\theta_1 = \frac{1}{l_t}\left(u_{c,GB} + u_{d,gb,v}\right) = \frac{P_{gb}}{l_t}\left(\frac{\alpha\sin\eta}{k_c} + \frac{1}{k_{d,gb}\sin\eta}\right) \quad (7)$$

$$\begin{aligned} M_{o,GB} &= 2P_{gb}h_t\cos\eta = 2P_{gb}l_t\sin\eta = \frac{2l_t^2}{\alpha/k_c + 1/k_{d,gb}\sin^2\eta}\theta_1 \\ &= \frac{2l_t^2}{\alpha/k_c + 1/k_{og,GB}}\theta_1 = k_{rg,GB}\theta_1 \end{aligned} \quad (8)$$

where h_t and η ($\tan^{-1}(h_t/l_t)$) are the vertical span and the inclined angle of BRB_GB, respectively. $k_{rg,GB}$ is the rotational stiffness provided by the GB outrigger system. The outrigger stiffness $k_{og,GB}$ is equal to $k_{d,gb}\sin^2\eta$ in the GB outrigger configuration. If $u_{d,ygb}$ is the axial yield deformation of BRB_GB, θ_y can be expressed as follows:

$$\begin{aligned} \theta_y &= \frac{k_{d,gb}u_{d,ygb}}{l_t}\left(\frac{\alpha\sin\eta}{k_c} + \frac{1}{k_{d,gb}\sin\eta}\right) \\ &= \frac{k_{d,gb}\sin^2\eta}{l_t}\left(\frac{\alpha}{k_c} + \frac{1}{k_{d,gb}\sin^2\eta}\right)\left(\frac{u_{d,ygb}}{\sin\eta}\right) \end{aligned} \quad (9)$$

When compared with Equations (2) and (3), the DM model can be used to model the structure with a GB outrigger by replacing k_d, k_t, and $u_{d,y}$ with $k_{d,gb}\sin^2\eta$, an infinity value, and $u_{d,ygb}/\sin\eta$, respectively. It is anticipated that the GB outrigger could conserve steel usage as the outrigger truss is not necessary. Furthermore, when the required BRB yield deformation is large, the long BRB in the GB outrigger configuration can be adopted easily. However, the BRB_GB may be required to span across more than one story, which may reduce usable floor areas. As indicated in Equation (8), the larger the value of η, the greater is $M_{o,GB}$. The seismic performance of structures with OB, BT, and GB outriggers can be estimated using the DM model (OB outrigger configuration) with modified parameters, as shown in Table 1, and its effectiveness is verified by the analysis results calculated using MBM models, which follow individual outrigger configuration details. The details of the MBM model for each outrigger configuration are introduced in the following sections. The DM model with an OB outrigger configuration is used to investigate the optimal outrigger elevation for minimizing maximum roof drift ($\theta_{\max}$) and core structure base overturning moment ($M_{c,\max}$).

4. Analysis Methods

4.1 Index definitions

In each BRB-outrigger configuration, the relationship between outrigger stiffness (including BRB axial stiffness) and perimeter column stiffness is critical. Therefore, two dimensionless indexes are newly defined for the parametric study. Instead of the index S_{bc} described in the previous study,[9] the outrigger effect (S_{cc}) is defined as the ratio of rotational stiffness provided by the outrigger when k_t and k_d are infinity ($k_c l_t^2/\alpha$) to the core structure's rotational stiffness (EI/h), and can be expressed as follows:

$$S_{cc}(\alpha) = \frac{l_t^2 h k_c}{\alpha EI},\ S_{cc07} = S_{cc}(0.7) = \frac{l_t^2 h k_c}{0.7EI} \quad (10)$$

The value of S_{cc} when α equals 0.7 (S_{cc07}, outrigger effect factor) is used to indicate the magnitude of the outrigger effect. The stiffer perimeter column (larger k_c value) and longer outrigger span (larger l_t value) can enhance the outrigger effect. For taller structures, the EI can significantly increase because of the larger seismic demand. Therefore, the S_{cc07} would be smaller for taller structures. In design practice, the k_c should be determined primarily by the gravity load demands, and the l_t determined by the architectural plan. Therefore, the outrigger effect factor S_{cc07} also reflects the suitability of adopting an outrigger in certain buildings. The structure with larger S_{cc07} value suggests that the efficiency of the mitigating seismic response would be higher when an outrigger system is adopted. In addition to the indexes R_{dc} and R_{bc} described in the previous study,[9] the outrigger stiffness ratio (R_{oc}) is also newly defined as the ratio of outrigger stiffness, k_{og}, to the perimeter column axial stiffness, k_c, and is expressed as follows:

Table 1. Parameters used in the DM model for each outrigger configuration

Configuration	Outrigger stiffness (k_{og})	k_t	k_d	$u_{d,y}$
OB outrigger	$k_{og,OB} = \frac{k_d k_t}{k_d + k_t}$	k_t	k_d	$u_{d,y}$
BT outrigger	$k_{og,BT} = k_{bt}$	∞	k_{bt}	$u_{bt,y}$
GB outrigger	$k_{og,GB} = k_{d,gb}\sin^2\eta$	∞	$k_{d,gb}\sin^2\eta$	$\frac{u_{d,ygb}}{\sin\eta}$

$$R_{oc} = \frac{k_{og}}{k_c}, \begin{cases} k_{og} = k_{og,OB} = 1/(1/k_d + 1/k_t), \text{ for OB outrigger configuration} \\ k_{og} = k_{og,BT} = k_{bt}, \text{ for BT outrigger configuration} \\ k_{og} = k_{og,GB} = k_{d,gb} \sin^2 \eta, \text{ for GB outrigger configuration} \end{cases} \quad (11)$$

R_{oc} indicates the stiffness provided by the outrigger system. After the perimeter column size is determined, R_{oc} can provide engineers with a rough estimate of the required BRB sizes and outrigger truss stiffness according to the selected R_{oc} value.

4.2 Analytical models

A total of seven types of analytical models with different structural plans and building heights were used for the parametric study. Figure 4 shows the floor framing plan of the floor with an outrigger for the analytical models. The two outrigger elevations are designed to resist horizontal loads in EW direction. The dead load, which is also the mass source, is 0.8 tonf/m^2. Table 2 shows the details of the analytical models. The values of EI were selected such that the fundamental vibration periods of the models without an outrigger (Core model) were close to 0.03 h. The R_{oc} values were fixed at 0.09, 0.45, 0.91, 1.36, 1.82, 2.27, and 2.73. The S_{cc07} values were set to be smaller for taller structure models. Table 2 and Figure 5 show the ranges and distributions of the S_{cc07} and R_{oc} values for each analytical model. The S_{cc07} values were properly selected to create a dense and uniform distribution, as shown in Figure 5. Based on the distributions shown in Figure 5, the analysis results in this study are valid when the S_{cc07} and R_{oc} range from 0 to 4 and from 0 to 3, respectively. For each analytical model, the values of k_c and k_{og} can be calculated based on the selected S_{cc07} and R_{oc} values from Equations (10) and (11), and the DM model can be constructed accordingly.

4.3 BRB yield deformation

The method of calculating the BRB yield deformation ($u_{d,y}$) has been introduced in the previous study.[9] The force-deformation relationship of the BRB in the analytical model is bilinear with a post-yield stiffness ratio of 0.01. The axial deformation of the BRB in the OB outrigger when the building laterally deforms in the first mode shape until the roof drift reaches θ_r is defined as the $u_{d,y}$. Figure 6 shows the distributions of $u_{d,y}$ with respect to S_{cc07} and α when R_{oc} is 0.5, 1, 2, and 3 for the cases when l_t = 12 m and θ_r = 1/750. The α that results with the largest $u_{d,y}$ is approximately 0.5-0.7, and is higher when the value of R_{oc} is smaller. The value of $u_{d,y}$ changes primarily with α. The stiffer outrigger (larger R_{oc} value) results in smaller $u_{d,y}$ values, and the value of S_{cc07} has less effect on $u_{d,y}$. Under the same θ_r, it appears that the outrigger elevation with

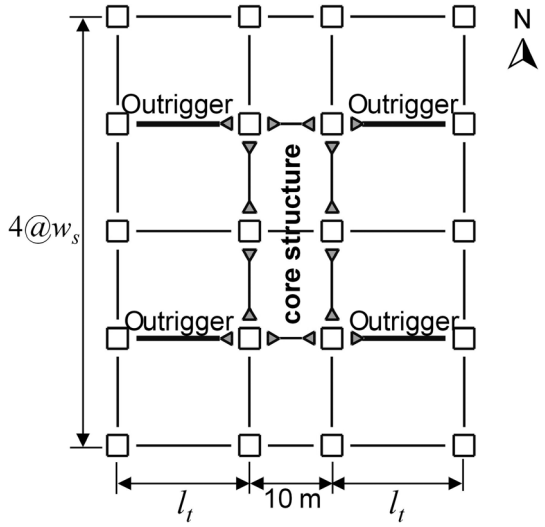

Figure 4. Floor framing plan of the analytical model

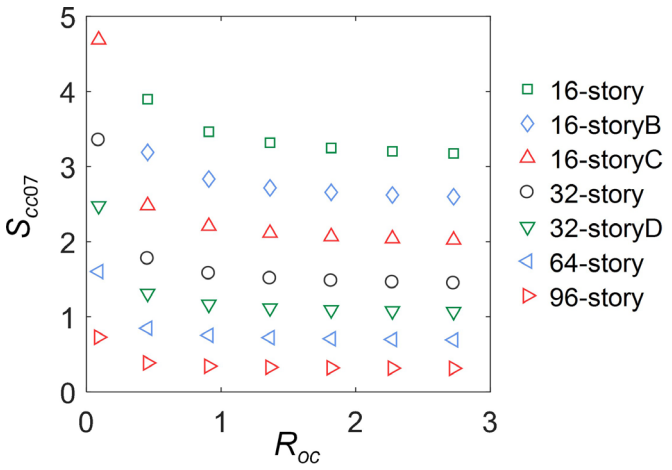

Figure 5. Distribution of S_{cc07} value with respect to R_{oc} for each analytical model

Table 2. Parameters of the analytical models

Model	h (m)	EI (kN-m^2)	l_t (m)	w_s (m)	S_{cc07}	Fundamental period of the core structure (sec)	R_{oc}
16-story	64	4.1 × 10^9	16	13	3.17-7.36	1.74	0.09-2.73
16-storyB	64	4.1 × 10^9	14.5	14	2.60-6.02	1.74	0.09-2.73
16-storyC	64	4.1 × 10^9	12.8	15.3	2.02-4.69	1.74	0.09-2.73
32-story	128	1.6 × 10^{10}	16	13	1.45-3.35	3.50	0.09-2.73
32-storyD	128	1.6 × 10^{10}	13.8	14.5	1.07-2.48	3.50	0.09-2.73
64-story	256	6.5 × 10^{10}	16	13	0.69-1.60	6.92	0.09-2.73
96-story	384	2.2 × 10^{11}	16	13	0.31-0.73	9.76	0.09-2.73

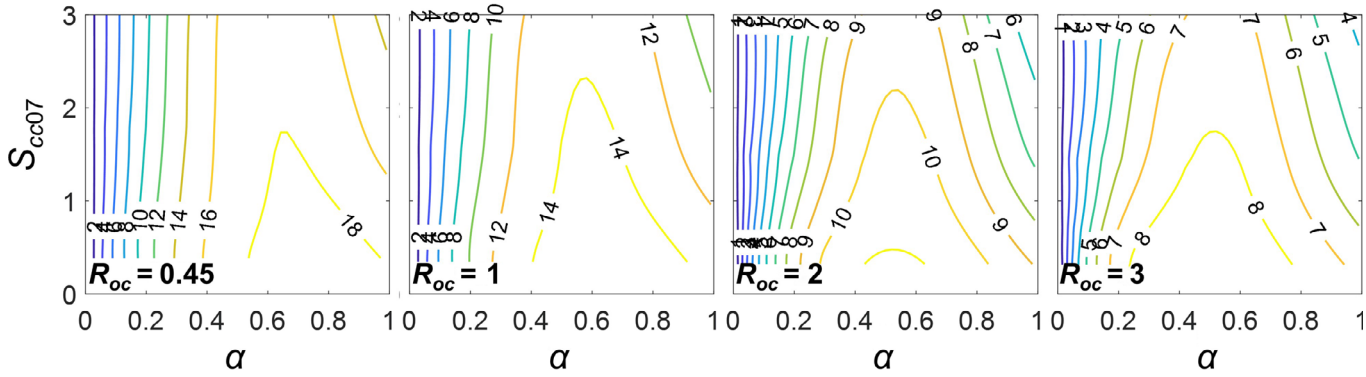

Figure 6. Distribution of $u_{d,y}$ with respect to α and S_{cc07} (unit: mm)

a larger $u_{d,y}$ value is more efficient for utilizing the axial deformation of the BRB in minimizing seismic response. For design practice, the $u_{d,y}$ is approximately 0.001 of the BRB length. Therefore, the $u_{d,y}$ shown in Figure 6 can be used to estimate the required BRB length at the preliminary design stage.

4.4 Spectral analysis

The SA procedure is used to evaluate the seismic performance of the BRB-outrigger system. To apply the SA to different outrigger configurations, the SA proposed in the previous study[9] has been modified. As the BRBs in a BT outrigger configuration may not yield simultaneously, this study uses the DM model to perform a modal pushover analysis (MPA)[12] using OpenSees to obtain a more accurate base shear and roof displacement relationship. Figure 7A shows the MPA result of the i^{th} mode, where $y_{top,i}$ is the roof displacement when the first BRB yields, K_i is the elastic modal stiffness, and $K_{eq,i}$ is the equivalent stiffness when the roof displacement reaches its maximum of $y_{\max,i}$. The lateral force pattern used in the MPA is assumed to keep the same elastic mode shape even when the BRB yields. The equivalent damping ratio ($h_{eq,i}$) of the i^{th} mode response with a ductility of μ_i is calculated as follows[13]:

$$h_{eq,i} = h_0 + \frac{1}{y_{\max,i}} \int_{y_{top,i}}^{y_{\max,i}} \frac{E_d(y)}{4\pi E_s(y)} dy, \quad \mu_i = \frac{y_{\max,i}}{y_{top,i}} \tag{12}$$

where $E_d(y)$ and $E_s(y)$ are the energy dissipated by the BRB-outrigger per loop, and the strain energy with a roof displacement of y (as shown in Figure 7B), respectively. h_0 (0.02) is the inherent damping ratio. The response spectrum is then adjusted, because of the increased damping ratio, using the reduction factor $D_{h,i}$ expressed as follows[14]:

$$D_{h,i} = \sqrt{\frac{1+\kappa h_0}{1+\kappa h_{eq,i}}}, \quad \begin{matrix} \kappa = 25 \text{ for observed ground motions} \\ \kappa = 75 \text{ for artifical ground motions} \end{matrix} \tag{13}$$

If $S_d(T,h_d)$ is the spectral displacement at period T and damping ratio h_d, the maximum roof displacement ($y'_{\max,i}$) of the response of the i^{th} mode can be estimated as follows:

$$y'_{\max,i} = D_{h,i} S_d\left(T_{eq,i}, h_0\right) \Gamma_i \phi_i(h) \tag{14}$$

where $T_{eq,i}$ is the equivalent vibration period, Γ_i is the i^{th} modal participation factor, and $\phi_i(h)$ is the roof displacement

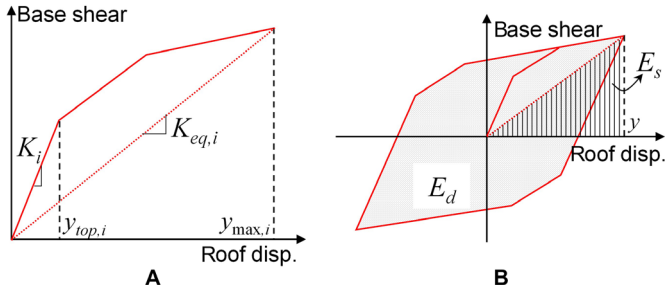

Figure 7. Relationship between (A) base shear and roof displacement obtained from MPA (B) E_d and E_s

in the i^{th} mode shape. The SA calculation is an iterative procedure and should be continued until the $y_{\max,i}$ used in computing $h_{eq,i}$ is sufficiently close to the $y'_{\max,i}$ obtained from Equation (14). It is anticipated that the yielding of BRBs only results in a marginal decrease in the stiffness of the entire structure. Thus, it is assumed that the modal superposition principle based on elastic mode shapes remains applicable.[12] The responses of the first four modes are calculated separately and then combined using the square root of the sum of the squares (SRSS) rule. If $\psi(x)$ is the lateral deformation at an elevation of x in the SRSS combined deformed shape, the maximum roof drift ($\theta_{\max}$) and the maximum overturning moment at the core structure base ($M_{c,\max}$) can be calculated as follows:

$$\theta_{\max} = \frac{|\psi(h)|}{h}, \quad M_{c,\max} = EI \left| \frac{d^2\psi(x)}{dx^2} \right|_{x=0} \tag{15}$$

4.5 Nonlinear response history analysis

The DM model constructed using OpenSees was also used to perform the NLRHA. The NLRHA was performed using eight ground motions (seven observed and one artificial), as shown in Figure 8. The spectral accelerations of the ground motions are scaled so that the mean of the spectral accelerations fits the design spectral acceleration within a range of $0.2T_1$ to $1.5T_1$, where T_1 is the first mode period.[15] A Rayleigh damping ratio of 0.02 for the first and second modes was applied for all NLRHA. The means of the NLRHA results obtained from the eight ground motions are used to verify the SA results.

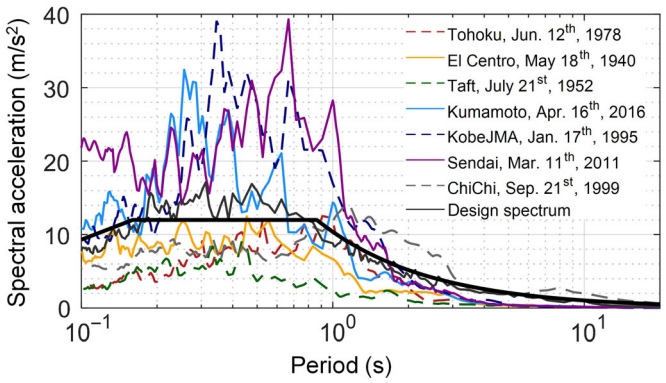

Figure 8. Response spectra of ground motions adopted in NLRHA

5. Analysis Results

5.1 Optimal outrigger elevations

As the BRB-outrigger applies a resisting moment to the core structure, the structure becomes stiffer when the outrigger effect is more significant. Therefore, the decrease in the first mode vibration period of the elastic system when compared with the Core model without an outrigger (D_{T1}) is used to estimate the effectiveness of the BRB-outrigger. The smaller D_{T1} value suggests that the outrigger effect is more significant. Figure 9A shows the distribution of α when the value of D_{T1} is smallest ($\alpha_{opt,T1}$) with respect to R_{oc} and S_{cc07}. The distribution of D_{T1} when the outrigger locates at $\alpha_{opt,T1}$ is shown in Figure 9B. When the value of S_{cc07} is larger, the ratio of the perimeter column axial stiffness to the core structure's flexural rigidity becomes larger. When the value of R_{oc} is larger, the ratio of the stiffness of the outrigger with BRB to the perimeter column axial stiffness becomes larger. Then, the outrigger effect is more significant as the D_{T1} is smaller. The $\alpha_{opt,T1}$ ranges from 0.5 to 0.8, and is lower when the values of R_{oc} and S_{cc07} are larger. Based on the analysis results, the relationship between $\alpha_{opt,T1}$, R_{oc}, and S_{cc07} can be approximately fitted using a polynomial with least square method as follows:

$$\begin{aligned}&\alpha_{opt,T1}(R_{oc},S_{cc07})\\&=0.9165-0.3672R_{oc}-0.05033S_{cc07}+0.188R_{oc}^2\\&\quad-0.006691R_{oc}S_{cc07}+0.005755S_{cc07}^2-0.03384R_{oc}^3\\&\quad+0.002815R_{oc}^2S_{cc07}+0.0004949R_{oc}S_{cc07}^2\\&\quad-0.0001824S_{cc07}^3\quad(0<S_{cc07}\le 4,\ 0<R_{oc}\le 3)\end{aligned}\tag{16}$$

Within the valid ranges of S_{cc07} and R_{oc}, the adjusted R-square value of Equation (16) is 0.94. The $\alpha_{opt,T1}$ calculated from using Equation (16) is shown in Figure 9A.

After the BRB yields, the BRB dissipates energy through its hysteretic response. The value of the equivalent damping ratio ($h_{eq,i}$) calculated using Equation (12) can be used to identify the energy dissipation efficiency of the BRB-outrigger system. As the first mode dominates the seismic response,[9] the equivalent damping ratio calculated from the first mode ($h_{eq,1}$) is used. The larger $h_{eq,1}$ value developed by the BRB-outrigger suggests the energy dissipation efficiency is higher. Figure 10A shows the distribution of the outrigger elevation when the value $h_{eq,1}$ is maximum ($\alpha_{opt,heq1}$) with respect to S_{cc07} and R_{oc}. The distribution of $h_{eq,1}$ when the outrigger

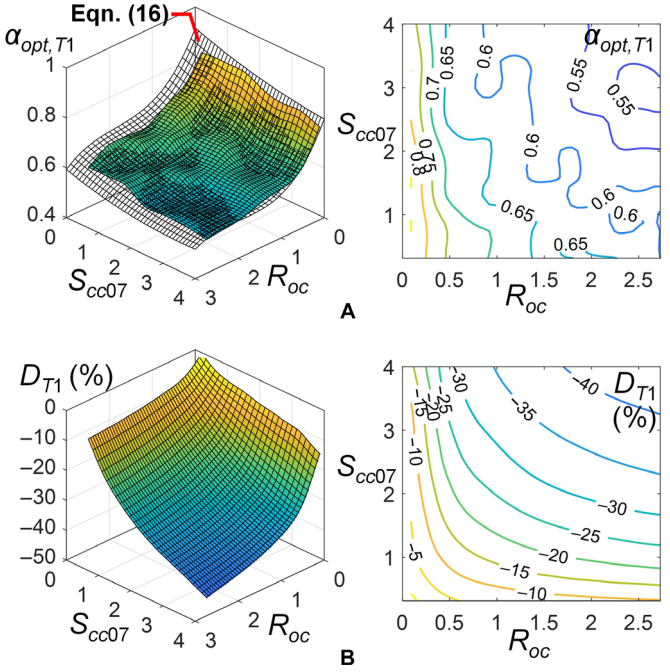

Figure 9. (A) $\alpha_{opt,T1}$ distribution and (B) D_{T1} distribution, with respect to S_{cc07} and R_{oc} calculated from SA

locates at $\alpha_{opt,heq1}$ is shown in Figure 10B. The larger R_{oc} and S_{cc07} values impose greater outrigger effect and thus result in a greater $h_{eq,1}$ value. The distribution of $\alpha_{opt,heq1}$ is similar to $\alpha_{opt,T1}$. The $\alpha_{opt,heq1}$ ranges from 0.6 to 0.9, and is lower when the values of R_{oc} and S_{cc07} are larger. Based on the analysis results, the relationship between $\alpha_{opt,heq1}$, R_{oc}, and S_{cc07} can be fitted using a polynomial with least square method as follows:

$$\begin{aligned}&\alpha_{opt,heq1}(R_{oc},S_{cc07})\\&=1.028-0.4112R_{oc}-0.06694S_{cc07}+0.2054R_{oc}^2\\&\quad-0.01297R_{oc}S_{cc07}+0.007359S_{cc07}^2-0.03614R_{oc}^3\\&\quad+0.002813R_{oc}^2S_{cc07}+0.003196R_{oc}S_{cc07}^2\\&\quad-0.0002686S_{cc07}^3\quad(0<S_{cc07}\le 4,\ 0<R_{oc}\le 3)\end{aligned}\tag{17}$$

Within the valid ranges of S_{cc07} and R_{oc} values, the adjusted R-square value of Equation (17) is 0.96. The $\alpha_{opt,heq1}$ calculated from using Equation (17) is shown in Figure 10A.

Figure 11 shows the distributions of the outrigger elevation when θ_{max} is minimum ($\alpha_{opt,\theta}$) with respect to R_{oc} and S_{cc07} calculated from SA and NLRHA. The distributions of θ_{max} when the outrigger locates at $\alpha_{opt,\theta}$ calculated from SA and NLRHA are shown in Figure 12. Both the SA and NLRHA results indicate that the larger values of R_{oc} and S_{cc07} result in a smaller θ_{max} response. The distribution of θ_{max} calculated from NLRHA and SA is similar. As the NLRHA results are sensitive to different ground motions, the $\alpha_{opt,\theta}$ calculated from NLRHA results does not exhibit a similar distribution to the SA results. However, both the SA and NLRHA results suggest that $\alpha_{opt,\theta}$ ranges approximately from 0.6 to 0.8. $\alpha_{opt,\theta}$ is smaller when the values of R_{oc} and S_{cc07} are larger, which is similar to $\alpha_{opt,T1}$ and $\alpha_{opt,heq1}$. Based on the SA results, the relationship between $\alpha_{opt,\theta}$, R_{oc}, and S_{cc07} can be fitted using a polynomial with least square method as follows:

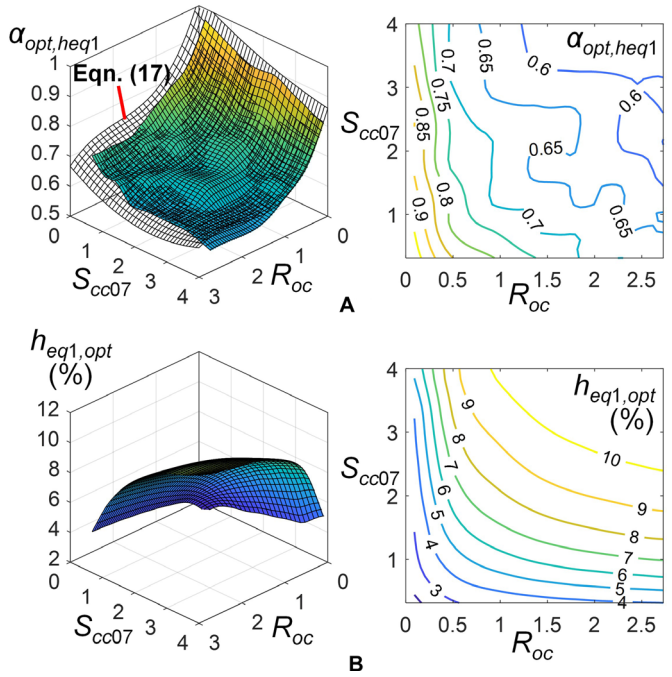

Figure 10. (A) $\alpha_{opt,heq1}$ distribution and (B) $h_{eq,1}$ distribution, with respect to S_{cc07} and R_{oc} calculated from SA

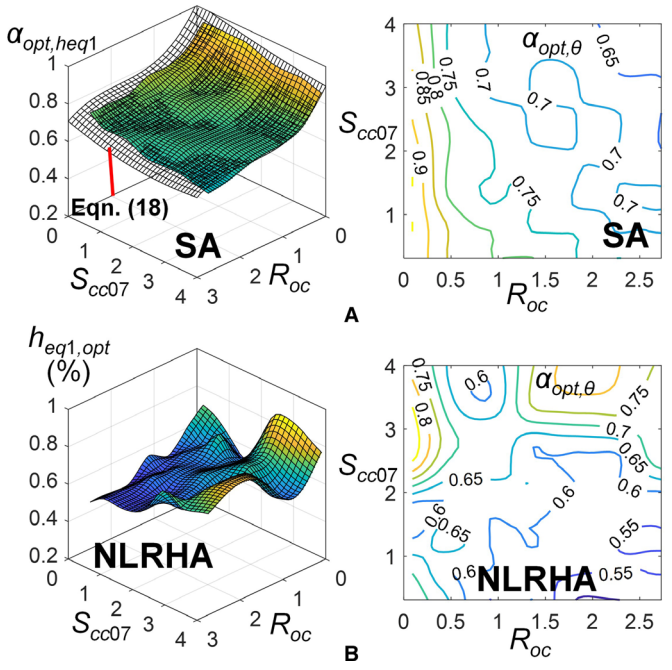

Figure 11. Distribution of $\alpha_{opt,\theta}$ with respect to S_{cc07} and R_{oc} calculated from (A) SA and (B) NLRHA

$$\begin{aligned}&\alpha_{opt,\theta}(R_{oc},S_{cc07})\\&=1.016-0.3824R_{oc}-0.04082S_{cc07}+0.2075R_{oc}^2\\&\quad-0.007177R_{oc}S_{cc07}+0.002457S_{cc07}^2-0.03809R_{oc}^3\\&\quad+8.228\times10^{-5}R_{oc}^2S_{cc07}+0.002544R_{oc}S_{cc07}^2\\&\quad+6.748\times10^{-5}S_{cc07}^3\quad(0<S_{cc07}\le4,\ 0<R_{oc}\le3)\end{aligned}\tag{18}$$

Within the valid ranges of S_{cc07} and R_{oc} values, the adjusted R-square value of Equation (18) is 0.94. The $\alpha_{opt,\theta}$ calculated from using Equation (18) is shown in Figure 11A.

Figure 13 shows the distributions of the outrigger elevation when $M_{c,\max}$ is minimum ($\alpha_{opt,Mc}$) with respect to R_{oc} and S_{cc07} calculated from SA and NLRHA. The distributions of $M_{c,\max}$ when the outrigger locates at $\alpha_{opt,Mc}$ calculated from SA and NLRHA are shown in Figure 14. The $M_{c,\max}$ calculated from NLRHA is similar to SA. The $M_{c,\max}$ decreases with increasing S_{cc07} and R_{oc} values. However, the $M_{c,\max}$ stops decreasing when S_{cc07} is greater than around 1-2 and when R_{oc} is greater than 1. The SA results indicate that $\alpha_{opt,Mc}$ drops to around 0.2 when R_{oc} and S_{cc07} are greater than approximately 0.5. However, the NLRHA results suggest that $\alpha_{opt,Mc}$ drops to around 0.3 when R_{oc} and S_{cc07} are greater than around 2 and 3, respectively. The differences between the SA and NLRHA results could be due to the SA calculation of $M_{c,\max}$ being based on elastic mode shape and linearly elastic force-deformation relation, and the NLRHA results could be sensitive to different ground motions. However, both the SA and NLRHA show the trend that the $\alpha_{opt,Mc}$ would be lower when the values of S_{cc07} and R_{oc} are larger. Based on the SA results, the relationship between the $\alpha_{opt,Mc}$, R_{oc}, and S_{cc07} can be fitted using a polynomial with least square method as follows:

$$\begin{aligned}&\alpha_{opt,Mc}(R_{oc},S_{cc07})\\&=1.583-1.421R_{oc}-0.5673S_{cc07}+0.6559R_{oc}^2\\&\quad+0.1473R_{oc}S_{cc07}+0.1358S_{cc07}^2-0.1134R_{oc}^3\\&\quad+0.00461R_{oc}^2S_{cc07}-0.02445R_{oc}S_{cc07}^2\\&\quad-0.01047S_{cc07}^3\quad(0<S_{cc07}\le4,\ 0<R_{oc}\le3)\end{aligned}\tag{19}$$

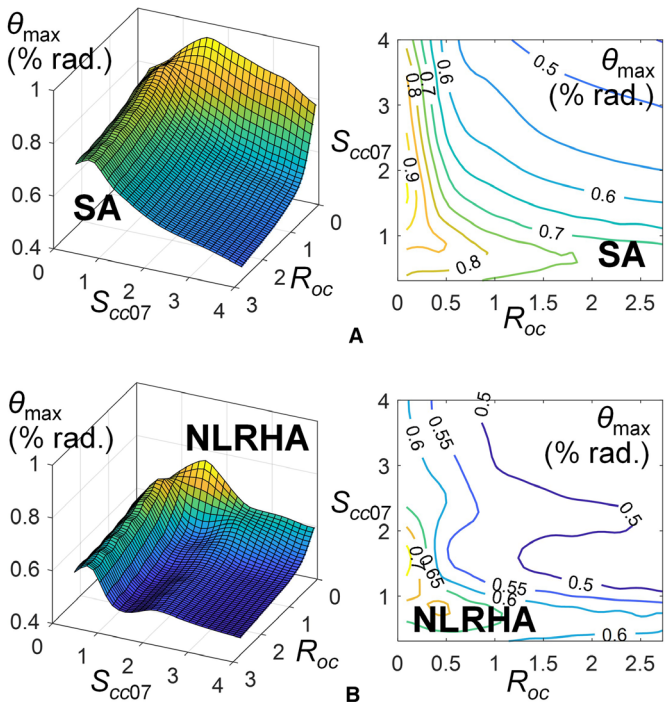

Figure 12. Distribution of θ_{max} with respect to S_{cc07} and R_{oc} calculated from (A) SA and (B) NLRHA

Within the valid ranges of S_{cc07} and R_{oc} values, the adjusted R-square value of Equation (19) is 0.76. The $\alpha_{opt,Mc}$ calculated from using Equation (19) is shown in Figure 13A. It should be noted that the polynomials shown in Equations (16)-(19) are only used to demonstrate the relationships between optimal outrigger elevations in order to achieve different optimal

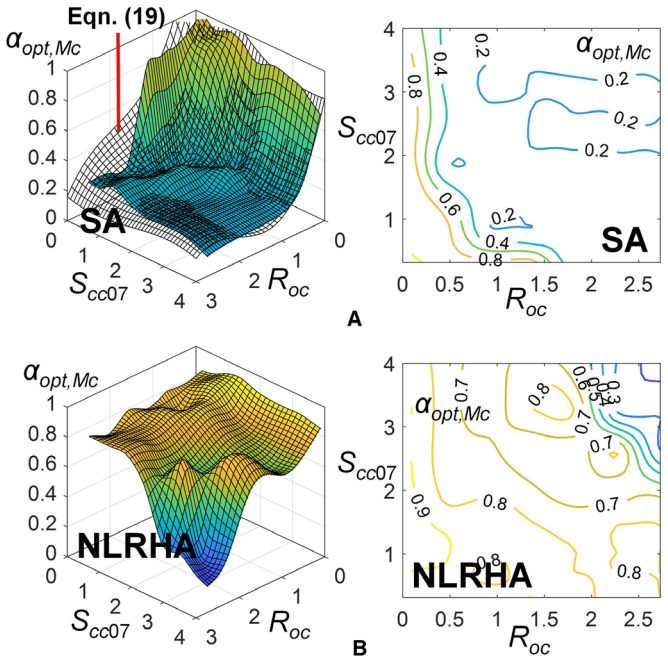

Figure 13. Distribution of $\alpha_{opt,Mc}$ with respect to S_{cc07} and R_{oc} calculated from (A) SA and (B) NLRHA

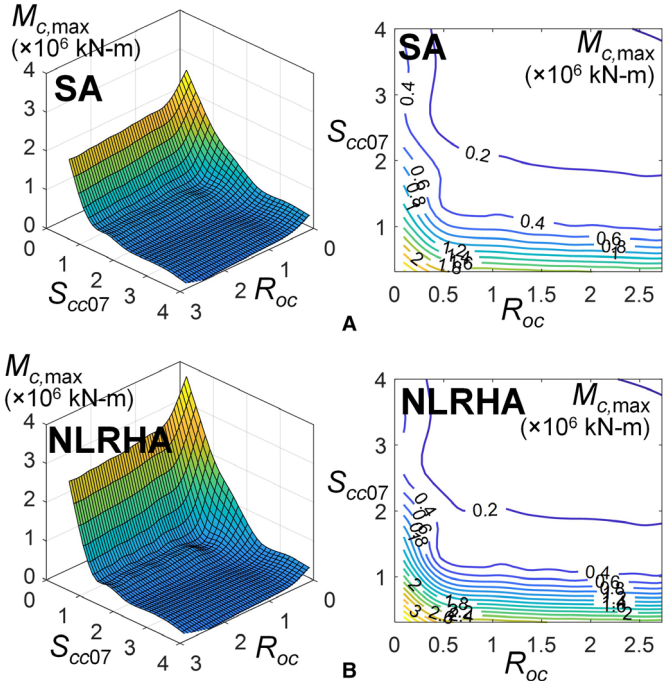

Figure 14. Distribution of $M_{c,max}$ with respect to S_{cc07} and R_{oc} calculated from (A) SA and (B) NLRHA

responses, which is introduced in the next section. Based on the analysis results, the ranges of $\alpha_{opt,T1}$, $\alpha_{opt,heq1}$, and $\alpha_{opt,\theta}$ are similar (0.6-0.8), but the range of $\alpha_{opt,Mc}$ (0.2-0.8) is much different from the others. This is because that the BRB-outrigger applies a resisting moment to the core structure to reduce seismic response. The core structure can result in greater rotational demand on BRB-outrigger at higher elevation, however, the axial stiffness provided from the perimeter column is smaller. Therefore, the BRB-outrigger elevation of 0.6-0.8 should be the best elevation to result in largest outrigger effect and to reduce θ_{max} response. On the other hand, as the maximum bending moment of core structure develops at the foundation, if the resisting moment applied by BRB-outrigger is closer to the core structure base, it is more efficient in reducing $M_{c,max}$ response.

5.2 Effects of outrigger effect factor and outrigger stiffness ratio

Figure 15 shows the reductions in θ_{max} (D_θ) when compared with the Core model when R_{oc} is 0.5, 1, 2, and 3 calculated from SA and NLRHA. The SA and NLRHA results are similar and indicate that the α that best reduces θ_{max} is approximately between 0.6 and 0.8, and is lower when the value of R_{oc} is larger (stronger outrigger effect). Under a fixed R_{oc} value, the larger S_{cc07} value leads to greater reductions in θ_{max} when α is higher than 0.5. This suggests that when α is lower than 0.5, θ_{max} cannot be effectively reduced by increasing the S_{cc07} value. The dashed lines in Figure 15 show $\alpha_{opt,T1}$, $\alpha_{opt,heq1}$, $\alpha_{opt,\theta}$, and $\alpha_{opt,Mc}$ calculated from Equations (16)-(19). The similar distributions of $\alpha_{opt,T1}$, $\alpha_{opt,heq1}$, and $\alpha_{opt,\theta}$ indicate that the optimal α to maximize outrigger effect, equivalent damping ratio, and to minimize θ_{max} is approximately 0.7-0.9. Furthermore, the $\alpha_{opt,T1}$, $\alpha_{opt,heq1}$, and $\alpha_{opt,\theta}$ distributions calculated from SA well match the D_θ distributions calculated from both SA and NLRHA. Figure 16 shows the reductions in $M_{c,max}$ (D_{Mc}) when compared with the Core model when R_{oc} is 0.5, 1, 2, and 3. Both the SA and NLRHA suggest that the larger S_{cc07} value results in greater reduction in $M_{c,max}$. The α that results in the greatest reduction in $M_{c,max}$ calculated from SA is lower than the one calculated from NLRHA. However, the $\alpha_{opt,Mc}$ can still provide satisfactory outrigger elevation to reduce the $M_{c,max}$ response, according to the NLRHA results. Furthermore, as shown in Figure 16B, the influence on D_{Mc} because of changes in α is insignificant when α is greater than 0.4. Therefore, the α selected from $\alpha_{opt,\theta}$, $\alpha_{opt,heq1}$, and $\alpha_{opt,T1}$ distributions can also provide satisfactory D_{Mc} response.

Based on the analysis results, both the D_θ and D_{Mc} responses indicate that the larger R_{oc} value offers a stiffer outrigger (stronger outrigger effect) and results in a smaller seismic response. However, the reductions in seismic responses are not proportional to the increasing R_{oc}. For example, when comparing the cases where R_{oc} increases from 1 to 2, the required outrigger stiffness k_{og} is doubled, but, the D_θ and D_{Mc} are increased by approximately 5% only. Therefore, to efficiently reduce seismic response utilizing a BRB-outrigger, selecting α approximately between 0.6 and 0.8, and an S_{cc07} value greater than 1 would be more efficient than increasing R_{oc}. In summary, based on the analysis results, to efficiently mitigate the seismic response, the optimal α is around 0.6-0.8, and the recommended values of S_{cc07} and R_{oc} are greater than 1 and around 0.5 and 1, respectively. Those recommended design parameters in order to minimize seismic responses are similar to the previous study,[9] in which the optimal design parameters were verified by performing a series of NLRHA. Figures 15 and 16 can be used as design charts to assist the designer in selecting the outrigger elevation and outrigger stiffness ratio for achieving the desired seismic response at the preliminary design stage. The examples with different outrigger configurations designed by utilizing the design charts are introduced in the following sections.

5.3 Design recommendation

The optimal values of α and R_{oc} in order to minimize seismic response are studied. Figure 17 shows the recommended

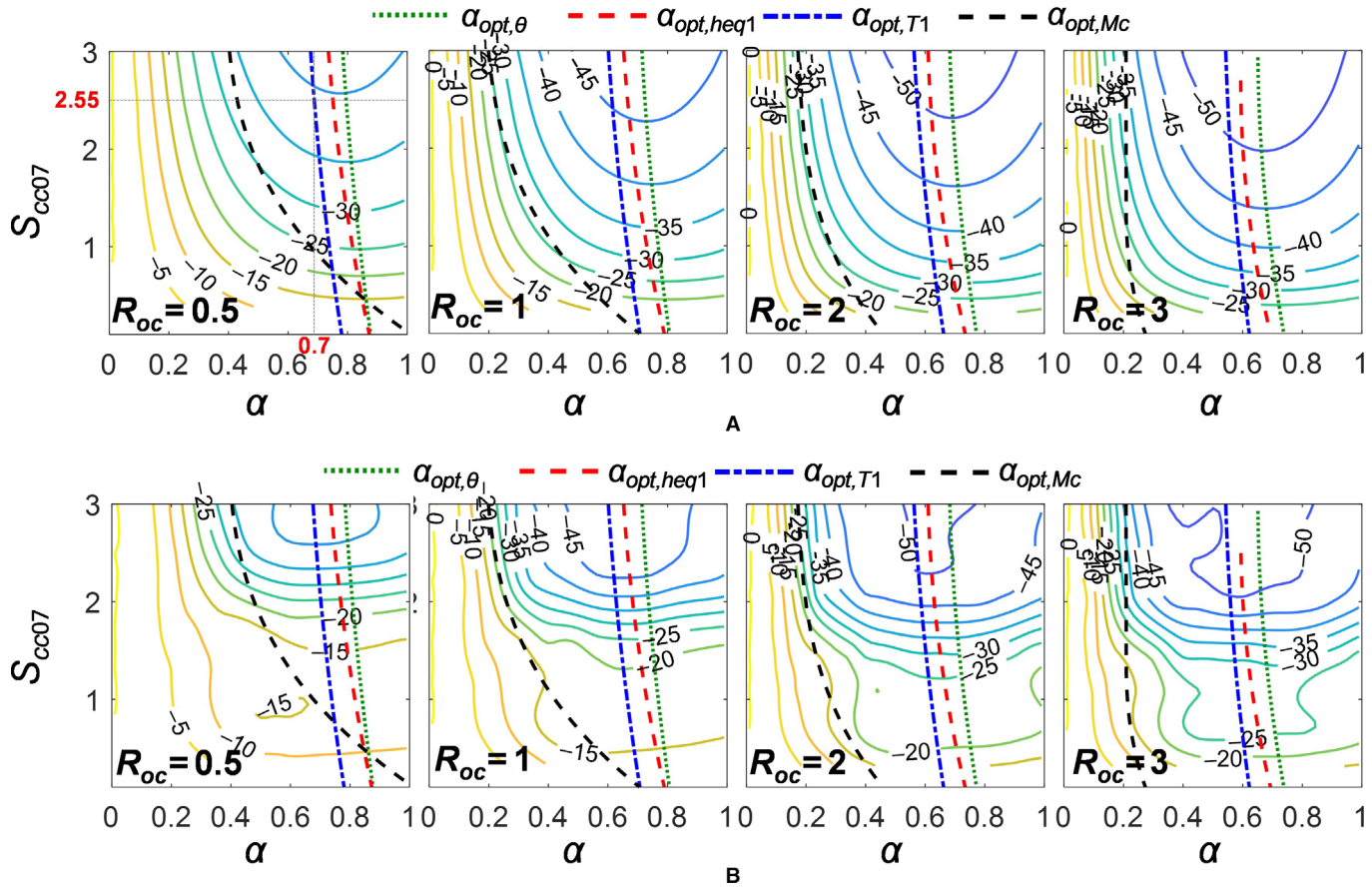

Figure 15. D_θ distribution chart calculated from (A) SA and (B) NLRHA

design flow chart. For design practice, the building lateral stiffness (core structure flexural rigidity, *EI*) should be mainly determined based on the code specifications. The perimeter column sizes (k_c) should be determined according to the floor framing plan and gravity load demands. The recommended design procedure is as follows,

1. If α is not restricted for architectural reasons, select α between 0.6 and 0.8, and calculate the S_{cc07} value.
2. Target R_{oc} value as large as possible within the range of 0.5 and 1.
3. Based on the selected R_{oc}, calculate the k_{og} and design the BRB and outrigger members. If the k_{og} is too large to design the BRB or outrigger members, select suitable BRB and outrigger member sizes and update the corresponding k_{og} and R_{oc} values.
4. Determine the BRB yield deformation (for example, 0.001 of the BRB element length). Then, perform the first mode MPA.
5. Confirm if the roof drift when BRB yields (θ_r) is within suitable range. If θ_r is too large (θ_r > 1/300),[9] decrease k_{og}. If θ_r is too small (θ_r < 1/800),[9] increase k_{og}.
6. After all the parameters are determined, perform the analysis and proceed to member design. As the outrigger effect results in additional force demands on the perimeter column, the perimeter column axial force demand should include the maximum BRB axial force capacity.

6. Effects of BRB-Outrigger Configurations

6.1 Introduction of example models

A 40-story model (h = 160 m) is used to demonstrate design examples for the structures with OB, BT, and GB outriggers. The structural plan is shown in Figure 4 with l_t and w_s equal to 12 m and 5 m, respectively. The core structure span is 5 m. The dead (mass source) and live loads are 0.8 tonf/m^2 and 0.3 tonf/m^2, respectively. The core structure flexural rigidity (*EI*) is 4 × 10^9 kN-m^2. Based on the dead and live load demands in the first story, the perimeter column with size of Box 900 × 900 × 75 mm, made from SN490 grade steel (material yield stress = 325MPa), was designed. The compressive demand-to-capacity ratio (DCR) of the perimeter column in the first story is 0.35. Therefore, the value of k_c is 309 375 kN/m, and the outrigger effect factor S_{cc07} of 2.55 can be calculated from Equation (10). The design details and the seismic performance of each configuration are introduced in the following sections. Based on the analysis results in previous sections, the value of R_{oc} is set to be approximately 0.45, and the α is set at 0.7. Therefore, the required outrigger stiffness (k_{og}) is approximately 139 219 kN/m, and the required $u_{d,y}$ is approximately 16-18 mm. As shown in Figures 15A and 16A, the case of R_{oc} = 0.45 and S_{cc07} = 2.55 when α = 0.7 suggests that the reductions in θ_{max} and $M_{c,max}$ are approximately 39% and 23%, respectively. With this condition, the seismic performance of structures with different BRB-outrigger configurations of OB, BT, and GB is compared.

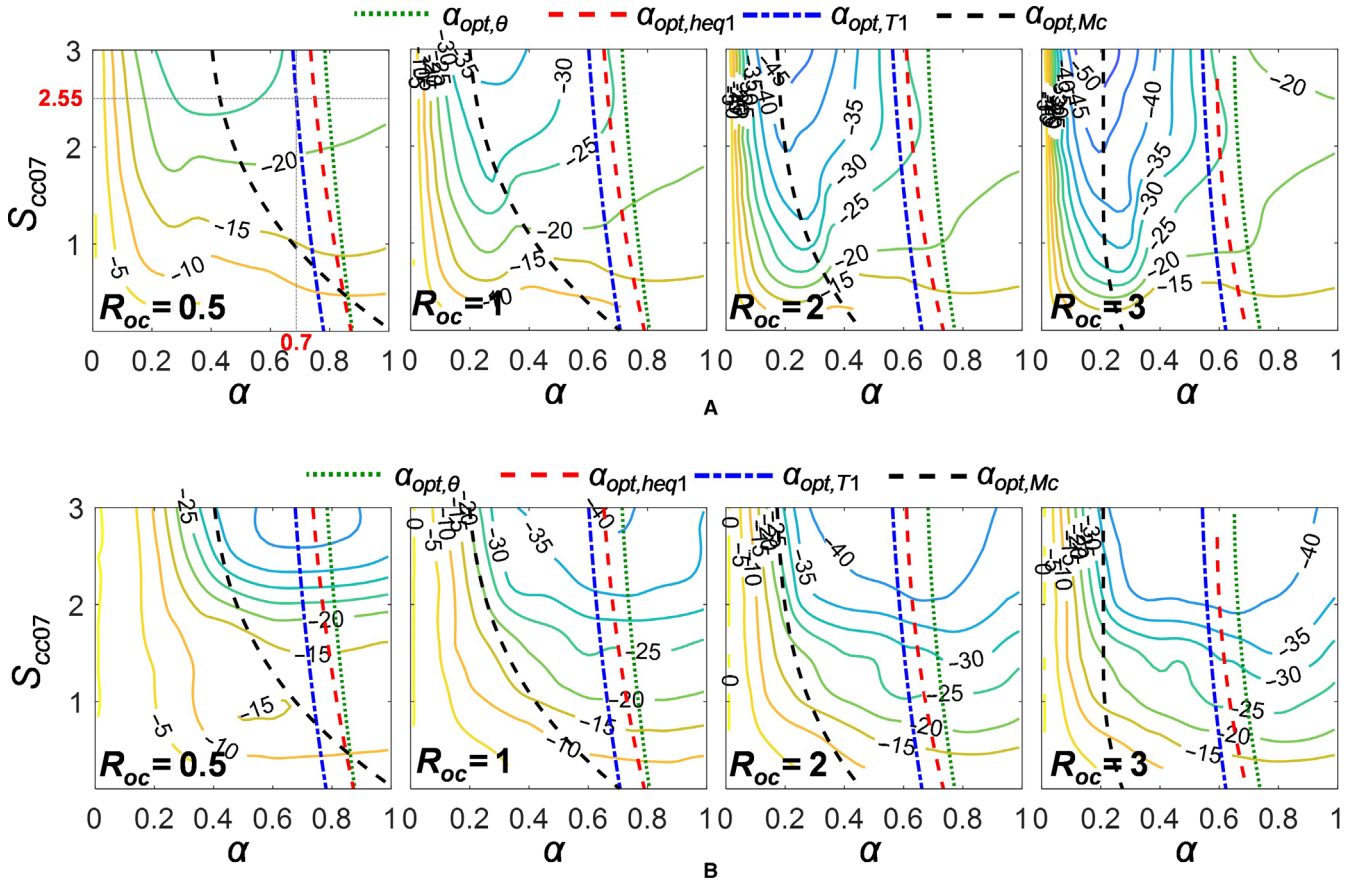

Figure 16. D_{Mc} distribution chart calculated from (A) SA and (B) NLRHA

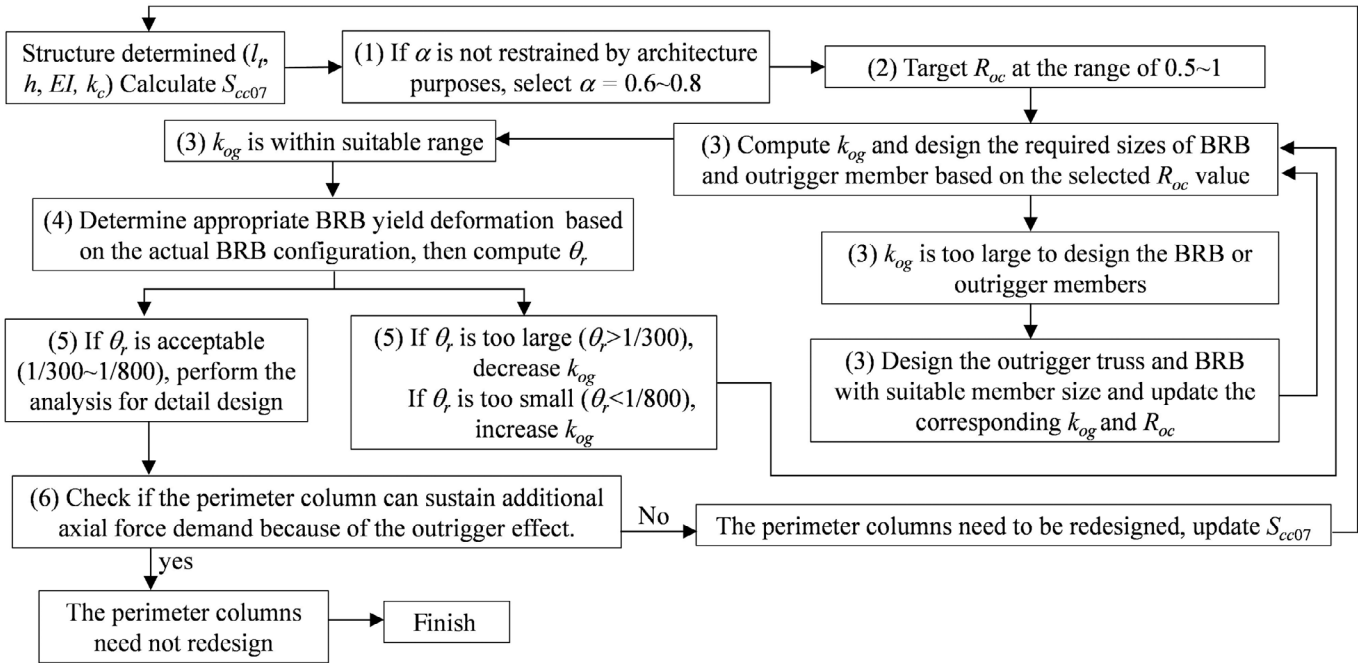

Figure 17. Flow chart of design recommendation

Figure 18A shows the design details of the OB outrigger. The top and bottom chords of the outrigger truss locate at the 28th and 27th floors, respectively. The two ends of the brace and column members in the outrigger truss are designed with moment connection detail. The connections between the top and bottom chords to the core structure are rigid connections. The top chord end near the perimeter column connects with the BRB, which is arranged vertically, with a length of 8 m. The bottom end of the BRB connects to the perimeter column at the 26th floor. Both two ends of the BRB are pinned connections. The 26th-floor beam is spliced adjacent to the lower BRB end. The value of k_t is 187 987 kN/m, which is calculated using OpenSees. Table 3 shows details of the BRB design in the OB outrigger configuration (BRB_OB). Figure 18B shows MBM model of OB outrigger. The members in the outrigger truss are modeled using beam column elements. The BRB_OB, which is modeled using a truss element, connects to the outrigger truss end at Node A and to the perimeter column at Node C. The perimeter column at the 28th floor level is separated at Node B, which shares the same coordinates with Node A but moves independently of Node A. The bilinear material model with a post-yield stiffness ratio of 0.01 is used for all the outrigger truss and BRB members in order to confirm if the structural members deform inelastically.

Figure 19A shows the details of the BT outrigger. The top and bottom chords with both ends of shear connection detail locate at the 28th and the 27th floors, respectively. The member size of the top and bottom chords are the same as those of the OB outrigger (BH 700 × 500 × 50 × 70 mm), but the column size in the outrigger truss is designed to be smaller (RH 700 × 300 × 13 × 24 mm). The two ends of the outrigger truss columns are designed with moment connection detail. Four identical BRBs (BRB_BT), are arranged along the BT outrigger with an equal span of 3 m, as shown in Figure 19A. The design details of the BRB_BT are presented in Table 3. Figure 19B shows the BT outrigger in the MBM model. The top and bottom chords are modeled using beam column elements. The ends at Node A, B, C, and D are free to rotate about the out-of-plane direction using the equalDOF command in OpenSees. The ideal inelastic behavior of the BT outrigger is to let the BRB yield first and then dissipate majority of the input seismic energy. Slight inelastic deformations in the top and bottom chords and the columns in the BT outrigger would be permitted. The bilinear material model with a post-yield stiffness ratio of 0.01 is used for all the elements in the OB outrigger in order to confirm if the structural members deform inelastically.

Figure 20A shows the details of the GB outrigger. The top and bottom ends of the BRB (BRB_GB) connect to the core structure at the 28th floor and to the perimeter column at the 26th floor, respectively. Both BRB_GB ends are pinned connections. The floor beams at the 26th and 28th floors are spliced adjacent to the BRB connections. The details of the BRB_GB design are presented in Table 3. As the floor beam at the 26th floor is required to sustain the maximum axial force developed in the BRB_GB and has to be stiff enough to

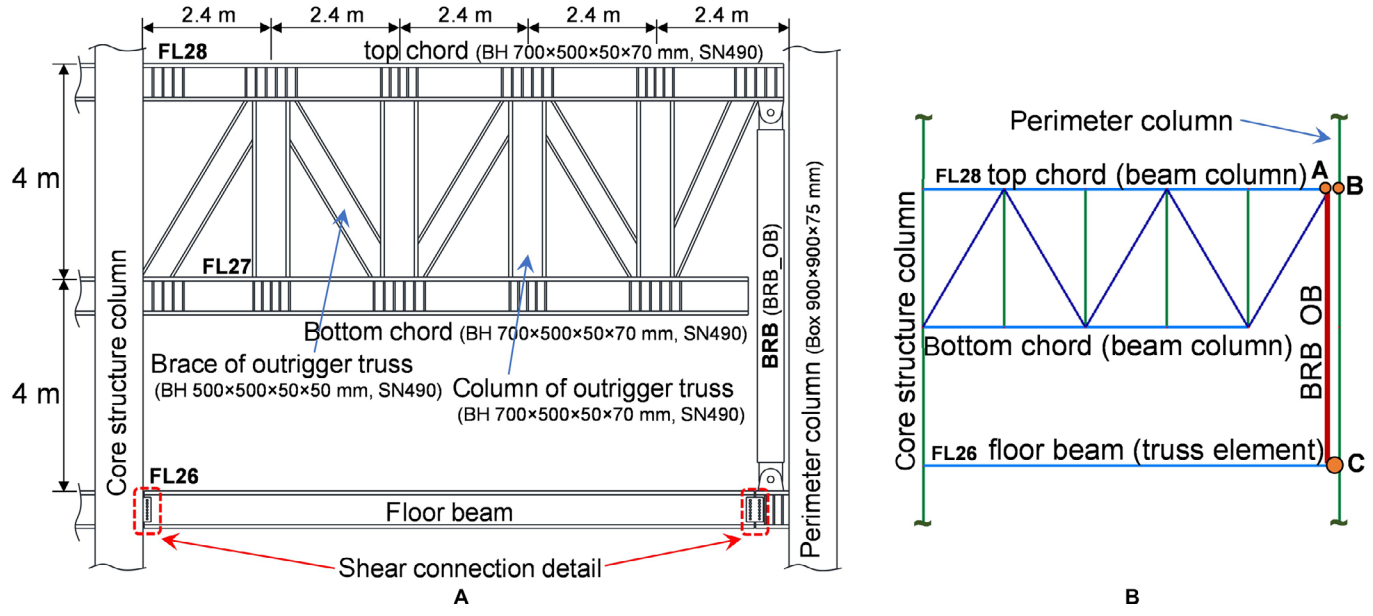

Figure 18. (A) Design detail and (B) MBM model of the OB outrigger

Table 3. Design details of the BRB in each outrigger configuration

BRB	Core material	Cross-sectional area (mm^2)			Segment length (mm)			Axial stiffness (kN/m)	Yield deformation (mm)	Yield axial force (kN)
		Core	Transition	Joint	Core	Transition	Joint			
BRB_OB	SN490	19 500	30 500	41 500	6500	110	640	538 518	11.8	6338
BRB_BT	SN490	22 275	34 925	47 575	2500	115	1135	1 200 962	6.0	7239
BRB_GB	SM570	27 600	40 080	52 560	6500	104	3846	51 6737	22.4	11592

prevent excessive axial deformation, the axial force demand for the 26th floor beam is estimated as 15 861 kN ($N_y \times 1.1 \times 1.3 \times 1.15 \times \cos\eta$, where N_y is the axial yield force of the BRB_GB, and the perimeters 1.1, 1.3, and 1.15 are the factors accounting for material overstrength, strain hardening, and compression strength adjustment, respectively). It is assumed that sufficient lateral support is provided on the 26th-floor beam. Therefore, size BH 820 × 400 × 22 × 50 mm, made from SN490 grade steel, can be designed with a compression DCR of 0.97. The axial stiffness of the

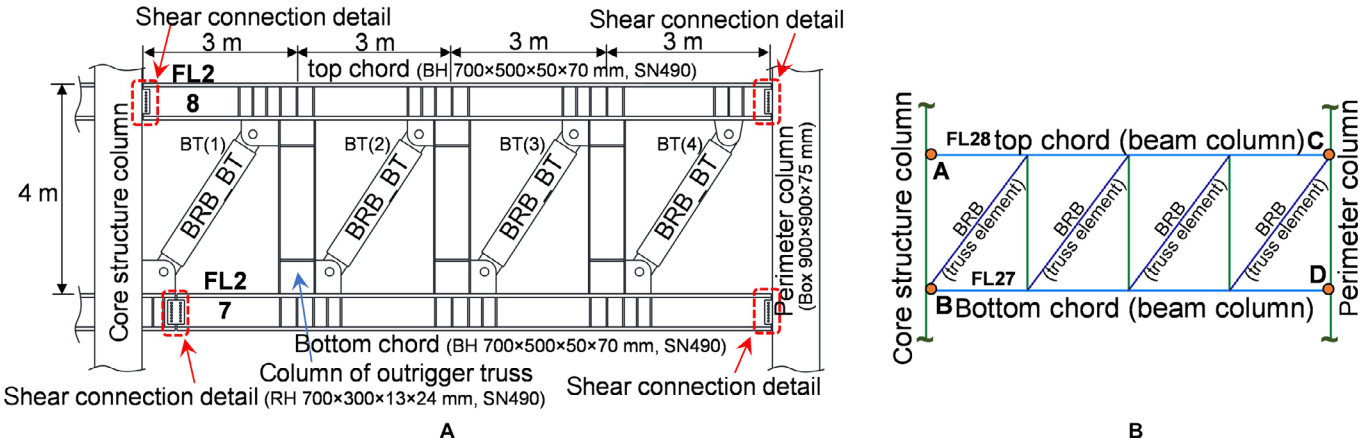

Figure 19. (A) Design detail and (B) MBM model of the BT outrigger

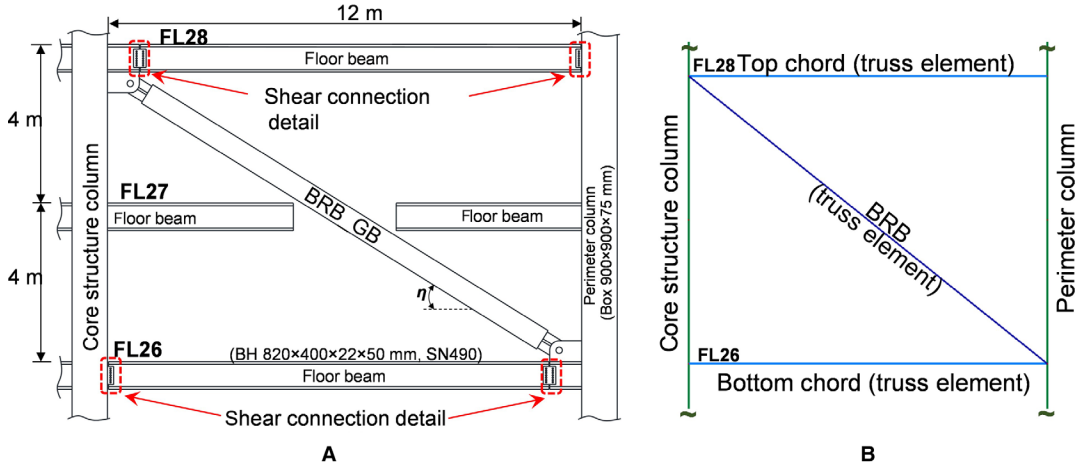

Figure 20. (A) Design detail and (B) MBM model of the GB outrigger

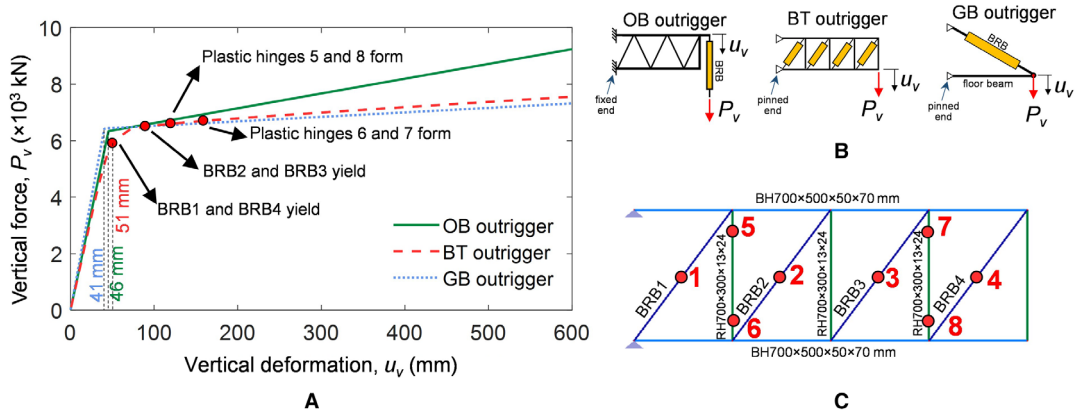

Figure 21. (A) Vertical force and vertical deformation relationship. (B) Illustrations for performing vertical pushover analysis for the OB, BT, and GB outriggers. (C) Illustration of plastic hinge locations of the BT outrigger

26th-floor beam is 2.6 times the axial stiffness of the BRB_GB in a horizontal direction. Thus, it should be stiff enough to prevent excessive axial deformation. Figure 20B shows the GB outrigger in the MBM model; the 27th-floor beam is not included. Both the BRB and floor beams are modeled using truss elements. The bilinear material model with a post-yield stiffness ratio of 0.01 was used for the BRB member.

6.2 Seismic response of the example models

Figure 21A shows the relationship between the vertical force applied at the outrigger end (P_v) and the corresponding vertical deformation (u_v) in each outrigger configuration calculated from the vertical pushover analysis using OpenSees. Figure 21B illustrates the vertical pushover analysis of each configuration. Based on the analysis results, the elastic outrigger stiffness (k_{og}) of the OB, BT, and GB outriggers is 139 344, 132 384, and 159 077 kN/m, respectively. The vertical deformation when BRB yields are 46, 51, and 40 mm for the OB, BT, and GB outriggers, respectively. Figures 21A and 21C show the sequence of BRB yielding and the flexural plastic hinges forming in the outrigger truss columns. BRB1 and BRB4 (Figure 21C) yield first when vertical deformation (u_v) reaches 51 mm (0.4% rad. deflection). BRB2 and BRB3 yield when u_v reaches 90 mm (0.8% rad. deflection). The flexural plastic hinges form at the two ends of outrigger truss columns when u_v reaches 120 and 159 mm (1% and 1.3% rad. deflection), respectively. The post-yield stiffness of the OB outrigger is slightly larger than that of the others. However, as the elastic stiffness and the yield deformation of the OB, BT, and GB outriggers are similar, it is anticipated that the structure with the different outrigger configurations would exhibit similar seismic response. Table 4 shows the parameters used in the DM model for the structure with different outrigger configurations. The value of 9×10^9 is used for infinity k_t in the DM model for BT and GB outrigger configurations.

Table 5 shows the first four mode vibration periods calculated from using DM and MBM models. The vibration periods calculated using the DM model are slightly larger than those from using the MBM model. Figure 22 shows the roof drift histories of the structures with OB, BT, and GB outriggers under BCJ-L2 ground motion (scale factor = 1). The roof drift history results obtained using DM and MBM models are close to each other. Furthermore, the roof drift responses between the three structures with different outrigger configurations are similar. The differences between the analysis results calculated using DM and MBM models could be due to the fact that the span of the core structure is not included in the DM model, the cantilever column in the DM model could not perfectly resemble the braced core structure in the MBM model, and the different distribution of mass along the building height in the DM and MBM model. The modal analysis and roof drift history results suggest that the DM model with modified parameters shown in Table 1 can be used to model the structure with BT and GB outrigger configurations. Furthermore, the structures with different BRB-outrigger configurations but sharing the same S_{cc07} and R_{oc} values exhibit very close seismic response. This indicates that the proposed indexes (S_{cc07} and R_{oc}) can effectively reflect seismic performance for a structure when any one of the OB, BT, or GB outrigger configurations is adopted.

Figures 23 and 24 show the maximum roof drift ($\theta_{\max}$) and the maximum overturning moment at the core structure base ($M_{c,\max}$) calculated from NLRHA with the original observed ground motions using DM and MBM models, respectively. Figure 25 shows the cumulative plastic deformation ratio $(R_{CPD})^{16}$ for the BRB in each outrigger configuration calculated from NLRHA using the MBM model. The locations of the four BRBs in the BT outrigger are shown in Figure 19A. The zero values of R_{CPD} indicate that the BRB deforms elastically. The analysis results show that $\theta_{\max}$ and $M_{c,\max}$ responses between the structures with OB, BT, and GB outrigger configurations are only slightly different. The model without an outrigger (Core model) generally exhibits greater $\theta_{\max}$ and $M_{c,\max}$ than the models with a BRB-outrigger. However, under

Table 4. Parameters used in DM model for the design example with different outrigger configurations

Configuration	k_{og} (kN/m)	k_t (kN/m)	k_d (kN/m)	$u_{d,y}$ (mm)	P
OB outrigger	139 344	187 987	538 518	11.8	0.01
BT outrigger	132 384	∞	132 384	51.0	0.01
GB outrigger	159 077	∞	159 077	40.4	0.01

Table 5. Vibration periods calculated using DM and MBM models for the design example with different outrigger configurations

		Vibration period (sec)			
Configuration	Model	1st mode	2nd mode	3rd mode	4th mode
OB outrigger	DM	4.383	0.840	0.316	0.160
	MBM	4.252	0.880	0.344	0.178
BT outrigger	DM	4.410	0.841	0.316	0.160
	MBM	4.390	0.890	0.344	0.178
GB outrigger	DM	4.312	0.835	0.316	0.160
	MBM	4.184	0.880	0.344	0.178

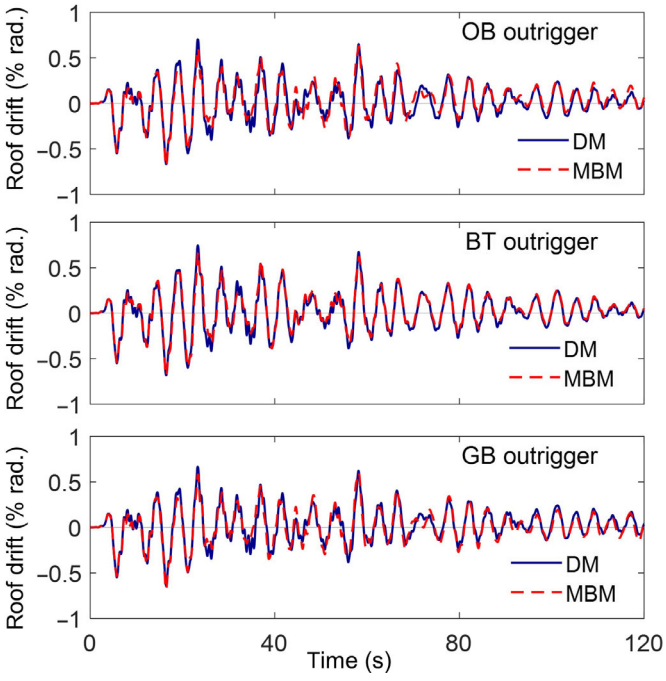

Figure 22. Roof drift history of models with OB, BT, and GB outrigger calculated using DM and MBM models

Tohoku, El Centro, Taft, and Kumamoto ground motions, the BRB-outrigger only slightly improves the seismic response when compared with the Core model. This is because the increased stiffness resulting from the outrigger effect might increase seismic demand, and the BRB deforms elastically (R_{CPD} = 0) or exhibits only slight inelastic deformation (low R_{CPD} values) and thus results in a low energy dissipation efficiency. Figure 26 shows the percentages of energy dissipated by the BRB (E_{BRB}) to the total input energy. The reductions in the $\theta_{\max}$ and $M_{c,\max}$ are greater when the value of E_{BRB} is larger. The reductions in $\theta_{\max}$ (the average of OB, BT, and GB outriggers), when compared to the Core model are approximately 27% and 50% under ChiChi and BCJ-L2 ground motions, respectively. Furthermore, the reductions in $M_{c,\max}$ (the average of OB, BT, and GB outriggers) when compared with the Core model are approximately 40% and 30% under ChiChi and BCJ-L2 ground motions, respectively. According to Figures 15 and 16, the SA results indicate that the reductions in $\theta_{\max}$ and $M_{c,\max}$ are around 39% and 23%, respectively. This suggests that the SA could provide appropriate estimations of the seismic response if the BRBs develop sufficient hysteretic responses. As shown in Figure 25, the R_{CPD} values also indicate the ductility demand for the BRB. The BRB_OB exhibits the largest R_{CPD} value as the vertical BRB arrangement imposes a large amount of axial deformation demand on the BRB_OB. The R_{CPD} values of the BRB_GB are smaller than those of the BRB_OB. However, the seismic response and the E_{BRB} of the models with OB and GB outrigger configurations are similar. This suggests that the GB outrigger configuration could be a better alternative configuration for preventing excessive ductility demand on the BRB, as a BRB with too large an R_{CPD} value could easily fracture before the end of an earthquake. For the BT outrigger, because of the outrigger arrangement, the ductility demands for the BRBs near the two outrigger truss ends (BRB_BT(1) and BRB_BT(4)) are greater than that for the BRBs in the midspan of the outrigger truss (BRB_BT(2) and BRB_BT(3)). In design practice, the sizes of the BRB in the BT outrigger configuration could be properly adjusted to reduce steel usage. For instance, BRB_BT(2) and BRB_BT(3) with low R_{CPD} values

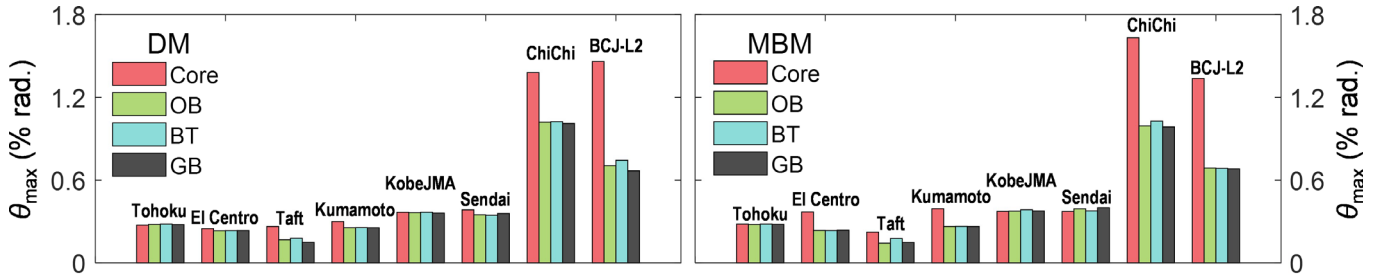

Figure 23. $\theta_{\max}$ responses calculated from NLRHA with the original observed ground motions

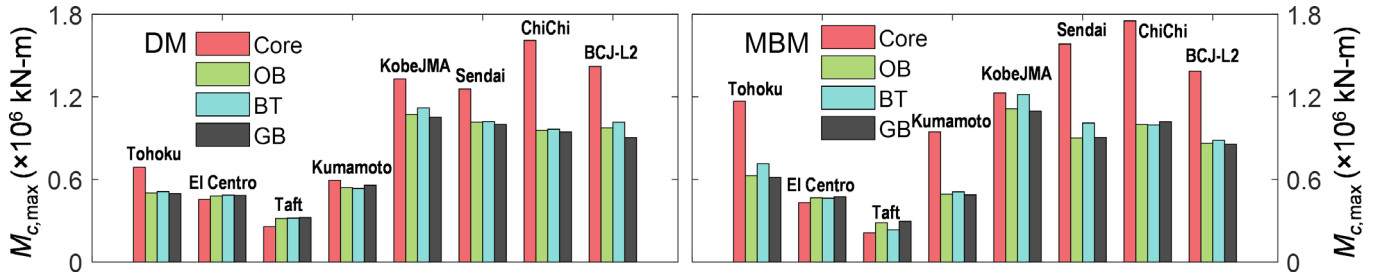

Figure 24. $M_{c,\max}$ responses calculated from NLRHA with the original observed ground motions

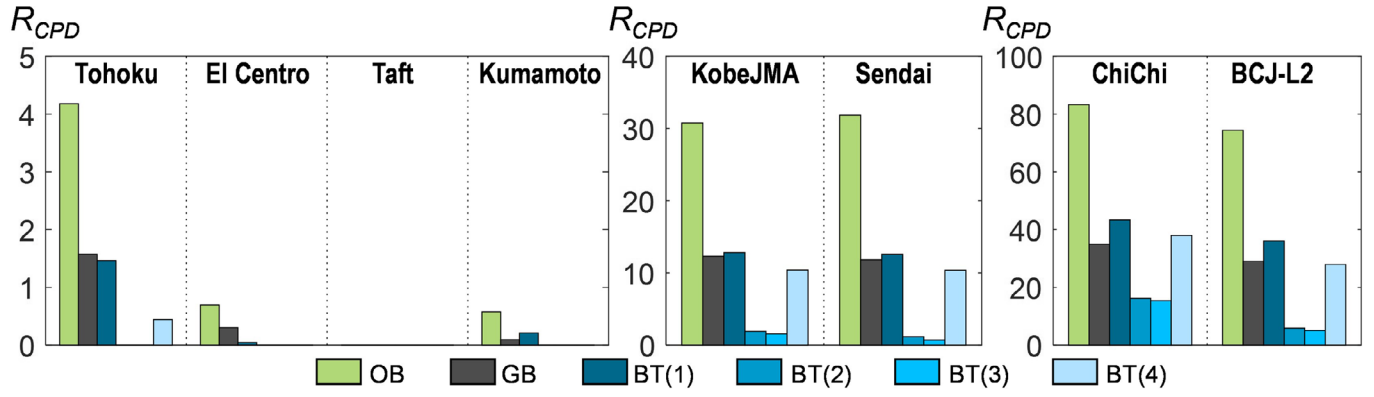

Figure 25. The R_{CPD} calculated from NLRHA with the original observed ground motions

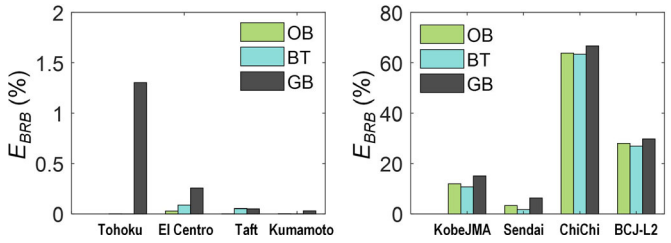

Figure 26. The E_{BRB} calculated from NLRHA with the original observed ground motions

Table 6. Steel usage for the OB, BT, and GB outriggers with single outrigger span

Configuration	Outrigger truss (tonf)	BRB (tonf)	Total (tonf)
OB outrigger	43.6	3.8	47.4
BT outrigger	20.6	11.2 (2.8 tonf for each BRB_BT)	31.8
GB outrigger	5.3 (including the 12 m-long floor beam)	9.2	14.5

in the design example could be replaced with ordinary elastic steel braces.

6.3 Comparison between OB, BT, and GB outrigger configurations

Table 6 shows the steel usage of the OB, BT, and GB outriggers (single span within the core structure and perimeter column) for the design example models. The weight of the 26th-floor beam in the GB outrigger, which is designed to sustain the maximum force developed by the BRB, is included. The OB outrigger consumes the most steel. Although the force demands on the OB outrigger truss members can be effectively limited by the maximum force capacity of the BRB_OB, the OB outrigger truss member sizes can be determined to create sufficient k_t value, instead of being determined by force demands. Furthermore, when the outrigger truss span (l_t) becomes longer, the required outrigger truss member size must be sharply increased. Therefore, the OB outrigger configuration would be suitable only when the outrigger truss span is short. However, the OB outrigger truss can be designed to occupy only one story; and only one BRB is required. The BT outrigger configuration requires more than one BRBs. Slight plastic deformations are allowed in the BT outrigger truss members to prevent too large a member size. Therefore, the design of the BT outrigger configuration is more flexible but more complicated than the OB outrigger configuration. Furthermore, as the BRB and outrigger truss act in parallel, the post-yield stiffness could be properly adjusted by selecting different sizes of the outrigger truss member. The larger post-yield stiffness ratio would be beneficial, as it avoids sudden stiffness drops, as seen in the OB and GB outrigger configurations when the BRB yields. The GB outrigger consumes the least amount of steel. However, the GB outrigger requires a very long BRB when the l_t is long, and the BRB_GB may be required to span more than two story heights to generate sufficient outrigger stiffness (k_{og}), which could reduce usable floor area. Based on the analysis results, all three outrigger configurations can achieve satisfactory seismic response and could be selected by designers to fit individual architectural requirements using the proposed indexes and design charts.

7. Conclusions

This study investigated the seismic performance of structures incorporating the BRB-outrigger as a lateral force resisting system using SA and NLRHA procedures. Three different BRB-outrigger configurations were proposed with common design indexes and charts. Based on the analysis results using the proposed simplified models, the conclusions of this study are as follows:

1. The outrigger elevation strongly affects seismic response. The ranges of outrigger elevation (α) in order to enhance outrigger effect, to increase equivalent damping ratio, and to reduce $\theta_{\max}$ response are 0.5-0.8, 0.6-0.9, and 0.6-0.8, respectively. The optimal outrigger elevation (α) should be approximately 0.6-0.8. Based on the NLRHA results, the maximum overturning moment at the core structure base can be efficiently reduced when the outrigger locates at its optimal elevation.
2. The outrigger effect factor S_{cc07} can be used to indicate the efficiency of utilizing the BRB-outrigger as a seismic resistance system to improve seismic performance. A large S_{cc07} value suggests the efficiency of mitigating the seismic response of the BRB-outrigger is higher. Based on the analysis results, the recommended value of S_{cc07} should be larger than 1.0.
3. The outrigger stiffness ratio R_{oc} indicates the required outrigger stiffness. A large R_{oc} value leads to better reductions in the seismic response but also increases the cost. According to the analysis results, when the value of S_{cc07} is greater than 1.0, selecting an outrigger elevation α of 0.6-0.8 should be the first priority. The R_{oc} is then selected to fit the desired seismic response.
4. When the outrigger locates at approximately $\alpha = 0.6$ to 0.8, and when the values of S_{cc07} and R_{oc} are greater than 1.0 and 0.5, respectively, both maximum roof drift ratio and maximum overturning moment at the core structure base can be reduced by approximately 20%-30%, if the BRBs develop full hysteretic responses.
5. Three different BRB-outrigger configurations were designed and calibrated using the proposed indexes and charts, and their seismic performance was investigated in this study. According to the analysis results, the proposed indexes (S_{cc07} and R_{oc}) can effectively reflect the seismic performance of a structure with a BRB-outrigger when any one of the OB, BT, and GB outrigger configurations is adopted.
6. From the viewpoint of BRB design, the OB and GB outrigger configurations are suitable when the outrigger span is short. The OB and BT outrigger configurations utilize the building interior space best. The GB outrigger could be the most economical solution as outrigger truss members are not necessary. All three BRB-outrigger configurations are capable of achieving the desired seismic response. Designers can select suitable BRB-outrigger configurations to fulfill both architectural requirements and economical design using the proposed design charts and indexes.

Disclosure

The authors have no conflicts of interest to declare.

References

1 Ali M, Sun KS. Structural developments in tall buildings: current trends and future prospects. *Architecture Science Review*. 2007;**50**:205–223.
2 Smith S, Salim I. Parameter study of outrigger-braced tall building structures. *Journal of the Structural Division*. 1981;**107**:2001–2014.
3 Viise J, Ragan P, Swanson J. BRB and FVD alternatives to conventional steel brace outriggers. Proceedings of the CTBUH Shanghai Conference, pp. 691–699, 2014.
4 Smith R, Willford M. The damped outrigger concept for tall buildings. *The Structural Design of Tall and Special Buildings*. 2007;**16**:501–517.
5 Huang B, Takeuchi T. Dynamic response evaluation of damped-outrigger system with various heights. *Earthquake Spectra*. 2017;**33**:665–685.
6 Chen Y, McFarland D, Wang Z, Spencer B, Bergman L. Analysis of tall building with damped outriggers. *J Struct Eng*. 2010;**136**:1435–1443.
7 Willford M, Smith R. Performance based seismic and wind engineering for 60 story twin towers in Manila. Proceedings of the 14th World Conference on Earthquake Engineering, Beijing, China, 2008.
8 Takeuchi T, Wada A. *Buckling-restrained Braces and Applications*. Tokyo, Japan: The Japan Society of Seismic Isolation (JSSI); 2017.
9 Lin PC, Takeuchi T, Matsui R. Seismic performance evaluation of single damped-outrigger system incorporating buckling-restrained braces. *Earthquake Eng Struct Dynam*. 2018;**47**:2343–2365.
10 Joseph L, Gulec K, Schwaiger J. Wilshire grand: outrigger designs and details for a highly seismic site. *International Journal of High-rise Buildings*. 2016;**5**:1–12.
11 McKenna F. Objected oriented finite element programming frameworks for analysis, algorithm and parallel computing. PhD thesis. University of California, Berkeley, 1997.
12 Chopra A, Goel R. A modal pushover analysis procedure for estimating seismic demands for buildings. *Earthquake Eng Struct Dynam*. 2002;**31**:561–582.
13 Newmark N, Rosenblueth E. *Fundamentals of Earthquake Engineering*. Englewood Cliffs, NJ: Prentice-Hall; 1971.
14 Kasai K, Fu Y, Watanabe A. Passive control systems for seismic damage mitigation. *J Struct Eng*. 1998;**124**:501–512.
15 *Minimum Design Loads for Buildings and Other Structures*. Reston, VA: American Society of Civil Engineers (ASCE); 2010.
16 *Seismic Provisions for Structural Steel Buildings*. Chicago, IL: American Institute of Steel Construction (AISC); 2016.

How to cite this article: Lin P-C, Takeuchi T. Seismic performance of buckling-restrained brace outrigger system in various configurations. *Jpn Archit Rev*. 2019:00:1–17. https://doi.org/10.1002/2475-8876.12120

Appendix. List of symbols

$D_{h,i}$: reduction factor for response spectrum
D_{Mc}: drop of the $M_{c,\max}$ when compared with the Core model without outrigger
D_{T1}: drop of the first mode vibration period of the elastic system when compared with the Core model without outrigger
D_θ: drop of the $\theta_{\max}$ when compared with the Core model without outrigger
E_d: energy dissipated by the BRB-outrigger per loop
EI: core structure flexural rigidity
E_s: strain energy of the system
h: building height
h_0: inherent damping ratio
$h_{eq,i}$: equivalent damping of the i^{th} mode response
$h_{eq,i}$: equivalent damping ratio of the i^{th} mode response
h_t: vertical span of the BRB in the GB outrigger configuration
k_{bt}: flexural stiffness of the BT outrigger
k_c: axial stiffness of perimeter column with length of h.
$k_{d,gb}$: axial stiffness of the BRB in the GB outrigger configuration
k_d: axial stiffness of the BRB in the OB outrigger configuration
$K_{eq,i}$: equivalent stiffness when the roof displacement reaches its maximum of $y_{\max},i$
K_i: elastic modal stiffness of the i^{th} mode
$k_{og,BT}$: flexural stiffness combined with outrigger truss and BRB in the BT outrigger configuration
$k_{og,GB}$: flexural stiffness provided by the GB outrigger
$k_{og,OB}$: flexural stiffness combined with outrigger truss and BRB in the OB outrigger configuration
$k_{rg,BT}$: rotational stiffness provided by the BT outrigger system
$k_{rg,GB}$: rotational stiffness provided by the GB outrigger system
$k_{rg,OB}$: rotational stiffness provided by the OB outrigger system
k_t: flexural stiffness of outrigger truss in the OB outrigger configuration
l_t: outrigger span
$M_{c,\max}$: maximum overturning moment at core structure base
$M_{o,BT}$: moment applied by the BT outrigger until the core structure rotation at outrigger elevation reaches θ_1
$M_{o,GB}$: moment applied by the GB outrigger until the core structure rotation at outrigger elevation reaches θ_1
$M_{o,OB}$: moment applied by the OB outrigger until the core structure rotation at outrigger elevation reaches θ_1
p: post-yield stiffness ratio of BRB in OB outrigger configuration
P_{gb}: axial force of the BRB in the GB outrigger configuration
S_{cc}: outrigger effect when α varies from 0 to 1
S_{cc07}: outrigger effect factor (when $\alpha = 0.7$)
S_d: spectral displacement
$T_{eq,i}$: equivalent vibration period of the i^{th} mode
$u_{bt,y}$: flexural deformation of the BT outrigger when BRB yields
u_{bt}: flexural deformation of the BT outrigger
$u_{c,BT}$: axial deformation of perimeter column below outrigger elevation in the BT outrigger configuration
$u_{c,GB}$: axial deformation of perimeter column below outrigger elevation in the GB outrigger configuration
u_c: axial deformation of perimeter column below outrigger elevation in the OB outrigger configuration
$u_{d,gb,v}$: vertical component of the axial deformation of the BRB in the GB outrigger configuration
$u_{d,y}$: axial yield deformation of BRB in the OB outrigger configuration
$u_{d,ygb}$: axial yield deformation of BRB in the GB outrigger system
u_d: axial deformation of the BRB in the OB outrigger configuration
u_t: flexural deformation of the outrigger truss in the OB outrigger configuration
$y_{\max,i}$: maximum roof lateral displacement
$y_{top,i}$: roof lateral displacement when BRB yields in the i^{th} mode shape
Γ_i: modal participation factor of the i^{th} mode
T_1: the first mode vibration period
α: ratio of outrigger elevation to building height
$\alpha_{opt,heq1}$: optimal outrigger elevation for maximizing the first mode equivalent damping ratio
$\alpha_{opt,Mc}$: optimal outrigger elevation for minimizing $M_{c,\max}$
$\alpha_{opt,T1}$: optimal outrigger elevation for maximizing outrigger effect
$\alpha_{opt,\theta}$: optimal outrigger elevation for minimizing $\theta_{\max}$
ϕ_i: mode shape of the i^{th} mode
η: inclined angle of the BRB in the GB outrigger configuration
μ_i: ductility ratio of the i^{th} mode response
θ_1: core structure rotation at the height of outrigger elevation
$\theta_{\max}$: maximum roof drift ratio
θ_r: roof drift ratio of core structure when BRB yields
θ_y: core structure rotation at the height of outrigger elevation when BRB yields
ψ: SRSS combined deformed shape

Graphical Abstract

The contents of this page will be used as part of the graphical abstract of html only.
It will not be published as part of main article.

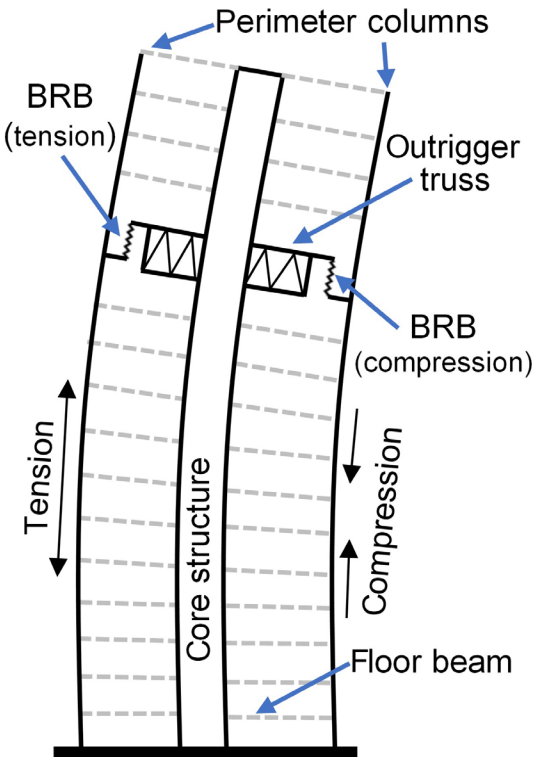

This research investigated the optimal design for structures with damped-outrigger incorporating BRB. Three different configurations of BRB-outrigger were introduced in detail. The seismic performances of the structures with different BRB-outrigger configurations were compared.